Available online at www.sciencedirect.com
SCIENCE DIRECT®
Geochimica et Cosmochimica Acta 70 (2006) 3325–3341
Geochimica
www.elsevier.com/locate/gca

Experimental study of germanium adsorption on goethite and germanium coprecipitation with iron hydroxide: X-ray absorption fine structure and macroscopic characterization

O.S. Pokrovsky [a,*], G.S. Pokrovski [a], J. Schott [a], A. Galy [b]

[a] *Aqueous and Experimental Geochemistry and Biogeochemistry, LMTG, UMR 5563 CNRS—Observatoire Midi-Pyrenées, 14 Avenue Edouard Belin, 31400 Toulouse, France*

[b] *Department of Earth Sciences, University of Cambridge, Downing Street, Cambridge CB2 3EQ, UK*

Received 18 October 2005; accepted in revised form 13 April 2006

Abstract

Adsorption of germanium on goethite was studied at 25 °C in batch reactors as a function of pH (1–12), germanium concentration in solution (10^{-7} to 0.002 M) and solid/solution ratio (1.8–17 g/L). The maximal surface site density determined via Ge adsorption experiments at pH from 6 to 10 is equal to 2.5 ± 0.1 μmol/m^2. The percentage of adsorbed Ge increases with pH at pH < 9, reaches a maximum at pH ~ 9 and slightly decreases when pH is further increased to 11. These results allowed generation of a 2-p*K* Surface Complexation Model (SCM) which implies a constant capacitance of the electric double layer and postulates the presence of two Ge complexes, >FeO–Ge$(OH)_3^0$ and >FeO–GeO$(OH)_2^-$, at the goethite-solution interface. Coprecipitation of Ge with iron oxy(hydr)oxides formed during Fe(II) oxidation by atmospheric oxygen or by Fe(III) hydrolysis in neutral solutions led to high Ge incorporations in solid with maximal Ge/Fe molar ratio close to 0.5. The molar Ge/Fe ratio in precipitated solid is proportional to that in the initial solution according to the equation $(Ge/Fe)_{solid} = k \times (Ge/Fe)_{solution}$ with $0.7 \leqslant k \leqslant 1.0$. The structure of adsorbed and coprecipitated Ge complexes was further characterized using XAFS spectroscopy. In agreement with previous data on oxyanions adsorption on goethite, bi-dentate bi-nuclear surface complexes composed of tetrahedrally coordinated Ge attached to the corners of two adjacent Fe octahedra represent the dominant contribution to the EXAFS signal. Coprecipitated samples with Ge/Fe molar ratios >0.1, and samples not aged in solution (<1 day) having intermediate Ge/Fe ratios (0.01–0.1) show 4 ± 0.3 oxygen atoms at 1.76 ± 0.01 Å around Ge. Samples less concentrated in Ge ($0.001 < Ge/Fe < 0.10$) and aged longer times in solution (up to 280 days) exhibit a splitting of the first atomic shell with Ge in both tetrahedral ($R = 1.77 \pm 0.02$ Å) and octahedral ($R = 1.92 \pm 0.03$ Å) coordination with oxygen. In these samples, octahedrally coordinated Ge accounts for up to ~20% of the total Ge. For the least concentrated samples (Ge/Fe < 0.001–0.0001) containing lepidocrocite, 30–50% of total co-precipitated germanium substitutes for Fe in octahedral sites with the next-nearest environment dominated by edge-sharing GeO_6–FeO_6 linkages ($R_{Ge-Fe} \sim 3.06$ Å). It follows from the results of our study that the largest structural change of Ge (from tetrahedral to octahedral environment) occurs during its coprecipitation with Fe hydroxide at Ge/Fe molar ratio ⩽0.0001. These conditions are likely to be met in many superficial aquatic environments at the contact of anoxic groundwaters with surficial oxygenated solutions. Adsorption and coprecipitation of Ge with solid Fe oxy(hydr)oxides and organo-mineral colloids and its consequence for Ge/Si fractionation and Ge geochemical cycle are discussed.

1. Introduction

Germanium, which belongs to the same group (IV) of the periodic table and has identical outer electron structure than silicon, has been often considered as a pseudoisotope of Si exhibiting a similar chemical behavior and substituting for it in silicate lattices (Goldschmidt, 1958; Cotton and Wilkinson, 1966). As a result Ge is an ideal candidate to trace both the continental and oceanic Si cycles (Froelich et al., 1985; Murname and Stallard, 1990; Froelich et al., 1992; Mortlock et al., 1993; Filippelli et al., 2000;

* Corresponding author. Fax: +33561332650.
E-mail address: oleg@lmtg.obs-mip.fr (O.S. Pokrovsky).

0016-7037/$ - see front matter © 2006 Elsevier Inc. All rights reserved.
doi:10.1016/j.gca.2006.04.012

Derry et al., 2005, 2006). This has been illustrated by Shemesh et al. (1989) who showed that diatoms exhibit little or no discrimination against Ge in the formation of biogenic opal thus making possible to use the Ge to Si ratio of this pair of elements recorded in diatoms through the last 500 ky to constrain paleovariations in continental weathering input (Murname and Stallard, 1990).

Careful comparison of silicon and germanium chemical properties, however, shows subtle but indisputable differences, with Ge exhibiting distinct lithopile, siderophile or organophile behavior depending on its environment (Bernstein, 1985; Pokrovski and Schott, 1998a,b). These specific properties are responsible for Ge geochemical cycles in the ocean and continental environments not being simple analogues of corresponding silica cycles. On the continents, for example, Ge/Si ratios measured in unpolluted streams ($0.3–1.2 \times 10^{-6}$) are almost always lower than the same ratios in the silicate bedrock (1.3×10^{-6}) they drain (Mortlock and Froelich, 1987). This requires Ge to be enriched in the secondary phases that form during the weathering of primary silicates. Aluminosilicates (Kurtz et al., 2002), Fe(III) oxy-hydroxides (Mortlock and Froelich, 1987; Pokrovsky and Schott, 2002) or humic acids in peats (Viers et al., 1997; Pokrovski and Schott, 1998b) have been proposed to be the soil reservoirs enriched in Ge. There is also a significant problem with interpreting the contemporary oceanic Ge/Si ratio because, unlike for Si, Ge mass balance in the ocean is still poorly constrained. It is generally assumed that the only sink for both elements is burial of biogenic opal (Tréguer et al., 1995), but the presently observed Ge/Si removal ratio yields by opal burial are $\sim 0.76 \times 10^{-6}$ whereas an extraction ratio of $\sim 1.3 \times 10^{-6}$ would be required for an ocean in steady state (King et al., 2000). In order to keep the ocean in steady state, an additional sink (often referred as the "missing sink") of $\sim 4 \pm 2 \times 10^{-6}$ mol Ge/yr is requested (Zhou and Kyte, 1991; Elderfield and Schultz, 1996). It has been recently proposed that the missing Ge sink can be linked to the selective uptake of Ge by authigenic Fe oxy-hydroxides phases in iron-rich margin sediments (King et al., 2000; McManus et al., 2003).

However, despite an important role ascribed to iron oxy-hydroxides in the control of germanium concentrations both in continental and marine environments, little is known about the mechanisms of Ge uptake by iron oxides via sorption/coprecipitation processes and the possible extent of this uptake. Moreover, because Ge, unlike Si, can easily increase its coordination number from 4 to 6 following, for example, its complexation with organic acids (Pokrovski et al., 2000) or its coprecipitation with Fe(III) oxy-hydroxides (Bernstein and Waychunas, 1987), it can be expected that germanium isotopes (i.e, $^{74}Ge/^{70}Ge$) can significantly fractionate compare to Si isotopes ($^{28}Si/^{30}Si$) during weathering and marine diagenesis.

Here, we have made concerted efforts aimed at rigorously characterizing germanium sorption on goethite and its coprecipitation with amorphous Fe(III) hydroxides. The chemical status of Ge associated with Fe hydroxides was thoroughly characterized using XAFS spectroscopy. It is expected that these new data will allow to better constrain Ge behavior in both continental and oceanic environments and to understand the reasons for Ge/Si fractionations.

2. Materials and methods

2.1. Adsorption experiments

Goethite powder (aggregates of crystals having a main size of 0.1 μm, determined by laser diffraction technique) was synthesized in the LEM laboratory (Nancy, France) following a procedure described by Cornell and Schwertmann (1996) and based on oxidative hydrolysis of $FeSO_4$. Its specific surface area was 23.2 m^2/g as determined by 3-point B.E.T. nitrogen adsorption technique. Batch adsorption experiments were performed in acid cleaned 30 mL polypropylene (PP) vials which were continuously agitated on a RotaMag® mixture at 25 ± 0.5 °C. Typical equilibration time of 1 week was used throughout the experiments. At the end of experiments, pH was measured, suspension centrifuged during 15 min at 2500 g, filtered through pre-cleaned 0.22 μm acetate cellulose sterile disposable filters, and acidified by bi-distilled HNO_3 prior the analysis. Solutions were prepared from ultrapure $NaNO_3$, HNO_3, NaOH and MilliQ water. Germanium stock solution was prepared by dissolving germanium dioxide (Fluka puriss. for electronic purposes, 99.99%) in deionized MilliQ water.

2.2. Coprecipitation experiments

Ge coprecipitation with iron oxy(hydr)oxide was performed in 30 mL PP vials via slow oxidation of 0.8–9.0 mmol/L Fe(II) nitrate or sulfate solutions in 0.1 M $NaNO_3$ or Na_2SO_4 by the atmospheric oxygen. Values of pH varied from 3 to 11 and the initial Ge concentration ($[Ge]_0$) varied from 1.4 to 1200 μmol/L. Depending on solution pH and intensity of stirring, a yellow fluffy precipitate was formed after 1–10 min after addition of $NH_4OH/NaHCO_3$ to initial $Fe(NO_3)_2/FeSO_4$ solution at pH 2. Kinetic experiments demonstrated stable amount of Ge removed after 10–100 min (see Section 3.3 below). Aging of precipitates at 25 °C in contact with solutions open to the atmosphere during 1–14 days did not produce any significant change of Ge and Fe aqueous concentrations.

Another method of Ge coprecipitation with iron hydroxide consisted of precipitating from initial Fe(III) solution with 0.90 mmol/L of Fe (made from $Fe(NO_3)_3$ in 0.1 M $NaNO_3$ at pH 2) by addition of 2% NH_4OH to pH ~ 6.5–7.5.

All precipitates were separated from solution by centrifugation during 10 min at 2500 g, rinsed in MilliQ water and dried 72 h at 60 °C. Their crystallinity was characterized via X-ray diffraction measurements using a G3000 INEL diffractometer.

2.3. Analyses

Solution pH was measured using a combination glass electrode (Mettler Toledo) calibrated on the activity scale with NBS buffers (pH 4.006, 6.865, and 9.180 at 25 °C). The precision of pH measurements was ±0.002 U (0.1 mV). Total germanium ($[Ge]_{tot}$) concentration was measured by flame atomic absorption using a Perkin-Elmer 5100 PC spectrometer in the concentration range of 30–800 μmol/L with an uncertainty of 2%. For Ge analyses in the concentration range of 1.4–140 μmol/L, colorimetric method with molybdenum blue was used (uncertainty of 2%). Finally, at very low concentrations ($[Ge] < 7$ μmol/L), dissolved germanium was determined by ICP-MS (Elan 6000, Perkin-Elmer) using ^{70}Ge and ^{74}Ge isotopes. Indium and rhenium were used as internal standards, and the international geostandard SLRS-4 (Riverine Water Reference Material for Trace Metals certified by the National Research Council of Canada) was used to check the validity and reproducibility of the analyses. The uncertainty of ICP-MS analyses was 10% at $[Ge] < 14$ nmol/L and 5% at $[Ge] \geqslant 14$ nmol/L. The three methods of Ge analysis employed in this study agreed within 5%. The Ge blank in our experiments was typically 30-60 pg. Total dissolved iron (Fe(II) + Fe(III)) was measured by flame atomic absorption using a Perkin-Elmer 5100 PC spectrometer in the concentration range of 3.6–90 μmol/L with an uncertainty of 2% and a detection limit of 0.9 μmol/L. Dissolved Fe(II) was analyzed spectrophotometrically using the ferrozine method (Viollier et al., 2000).

The MINTEQA2 computer program (Allison et al., 1991) was used to calculate the equilibrium species distribution in the $Ge(OH)_4$–H_2O–NaCl system. This program combines surface reaction equilibria, homogeneous solution equilibria, and mass balance calculations Aqueous species stability constants were taken from Pokrovski and Schott (1998b). The simplest surface speciation model, a single site, two-pK constant capacitance model (CCM) was used to model Ge adsorption on goethite.

2.4. X-ray absorption spectroscopy

XAFS spectra (including the X-ray absorption near edge structure region or XANES, and the extended X-ray absorption fine structure region or EXAFS) of selected adsorption and coprecipitation samples (1.4×10^{-3} mol/L $\leqslant [Ge] \leqslant$ 50 mol%) and germanic acid aqueous solutions ($[Ge_{aq}] = 0.005$–0.02 mol/L) were collected at ambient (20 ± 2 °C) and liquid-helium cryostat (~11 K) temperatures in the fluorescence or transmission modes (depending on Ge concentration) at the Ge K-edge (~11.1 keV) over the energy range 10.8–12.3 keV on ID26 and FAME beamlines at the European Synchrotron Radiation Facility (ESRF, Grenoble, France). The storage ring was operated at 6 GeV in multibunch mode with a 200–150 mA current during runs at ID26 and in 16-bunch mode with a 90–60 mA at FAME. The beam energy was selected using a Si(220) double crystal monochromator. The fluorescence spectra were collected using either a Silicon photo-diode (ID 26) or a 30-element Ge Canberra detector (FAME). The samples were placed in a Teflon cell with two 25-μm Kapton-film windows. The spectra acquisition procedure was similar to those described in Pokrovski et al. (2005) and Pokrovsky et al. (2004, 2005). Two to four scans (~55 min/scan data collection time each) for each sample were collected and averaged together. Germanium dioxides powders (quartz-like and rutile-like GeO_2) were used as model compounds for Ge local environment and their fluorescence spectra were recorded in similar conditions to our samples.

Data analysis was performed with the Athena and Artemis packages (Ravel and Newville, 2005) based on FEFFIT (Newville, 2001) and FEFF (Ankudinov et al., 1998) programs. Details about spectral reduction can be found in Pokrovski et al. (2005). To obtain structural information, fits were performed in the R-space on both real and imaginary parts of one or several Fourier Transform contributions. The fitted parameters include the identity of the backscattering atoms (e.g., O, Ge, or Fe), Ge-neighbor distance (R) and coordination number (N), and the Debye-Waller factor (σ^2) for a given scattering path. In addition to these structural parameters, a single non-structural parameter, Δe, was varied to account for its estimate made by FEFF. Typically Δe is defined as the difference in threshold energy calculated by FEFF and that measured in experiment. In order to (1) diminish correlations between N and σ^2 and (2) account more thoroughly for light-versus-heavy neighbors and multiple scattering events, fits were performed simultaneously with k-weightings of 1, 2 and 3 and the obtained values of structural parameters were averaged. Raw EXAFS spectra were also fitted with multiple shells; they produced values of structural parameters similar to those extracted from fits of filtered signals. Theoretical backscattering amplitude and phase-shift functions for Ge–O, Ge–Fe, Ge–Ge, Ge–H single and multiple scattering paths were computed with the FEFF 8 ab initio code (Ankudinov et al., 1998), using GeO_4–FeO_6 (±H) model clusters. The amplitude reduction factor (S0) used in modeling of experimental samples was set at 0.86 ± 0.08 as found by fitting EXAFS spectra of Ge-oxides. The anharmonicity of the pair-distribution function for the Ge 1st shell was checked using the cumulant expansion method but found negligible: the values of third- and fourth-order cumulants (c_3 and c_4) always converged to zero within errors. The influence of possible multiple scattering (MS) events within the Ge first coordination shell on the EXAFS spectra was also tested using the FEFF code, assuming local T_d and O_h geometries around Ge, as found in the model compounds investigated (see Section 3.4).

3. Results and discussion

3.1. Adsorption

All experiments on adsorption and coprecipitation are listed in the Electronic Annex. Like most adsorption processes, the interaction of aqueous Ge with goethite surface is quite fast: for typical experimental conditions (6.6 g/L of solid, pH 8.5), the stable Ge concentration in solution is achieved within 100–1000 min (Fig. 1). Adsorption was found fully reversible because, upon changing pH from acid to alkaline conditions and in backward direction, initial Ge concentration in solution was recovered.

"Langmurian" adsorption isotherms obtained at constant pH and variable $[Ge]_{aq}$ are presented in Fig. 2. For four pH values (6.75, 7.25, 7.8, and 9.6) and two solid concentrations (~4 and 8 g/L), the maximal surface sites density is estimated to be 2.5 ± 0.1 μmol/m^2. This is comparable with maximal Fe sites density on most common goethite face as computed by Pivovarov (1997) from crystallographic data.

The pH-dependent adsorption edges for germanium on goethite at initial [Ge] of 344 μmol/L are depicted in Fig. 3. The percentage of adsorbed Ge increases with pH at $2 \leqslant pH \leqslant 9$, reaches a maximum at $pH \sim 9$, and decreases at $pH > 9$. At lower [Ge], the maximum adsorption occurs at lower pH: for example, more than 95% of the total aqueous Ge is already adsorbed at $pH \geqslant 4$ for initial [Ge] of 0.14–1.4 μmol/L (Fig. 4).

3.2. Surface complexation modeling of adsorption

Germanium complexation with iron centers on goethite surface can be represented with two reactions corresponding to the two dominant species of germanic acid in solution ($Ge(OH)_4^0$ and $GeO(OH)_3^-$):

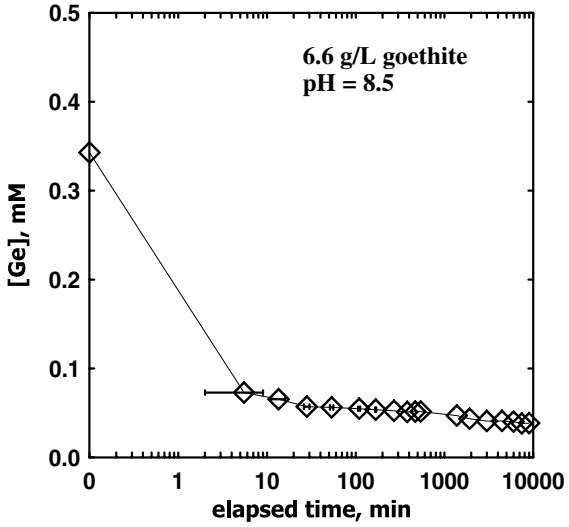

Fig. 1. Concentration of germanium in solution in contact with goethite as a function of time. The adsorption equilibrium is achieved within 100–1000 min. The solid line is an interpolation of the data.

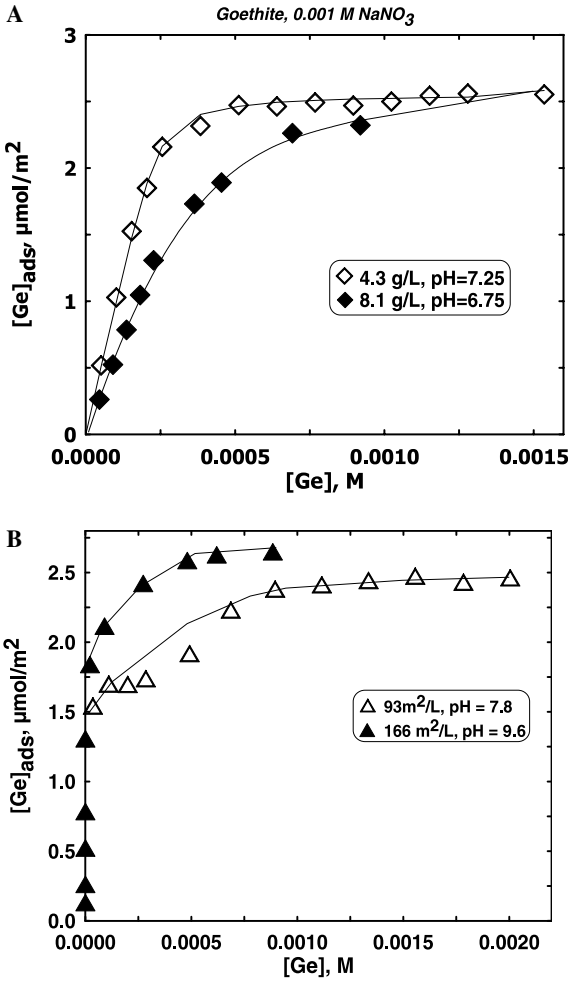

Fig. 2. Ge adsorption on goethite in 0.001 M $NaNO_3$ at 25 °C and constant pH. (A) Open diamonds, pH 7.25, 99 m^2/L; solid diamonds, pH 6.75, 188 m^2/L. (B) Open triangles, pH 9.6, 166 m^2/L, solid triangles, pH 7.8, 93 m^2/L. The solid lines were generated using SCM described in this study (0.75 F/m$_2$; $\log K_1$ (>FeO–$Ge(OH)_3^0$ = 5.4; $\log K_2$ (>FeO–$GeO(OH)_2^-$) = −2.9). The error bars are within the size of symbols.

$$Ge(OH)_4^0(aq) + >FeOH^0 = >FeO\text{–}Ge(OH)_3^0 + H_2O \quad (1)$$

$$Ge(OH)_4^0(aq) + >FeOH^0 = >FeO\text{–}GeO(OH)_2^- + H_2O + H^+ \quad (2)$$

Accordingly, two dominant species forming at the goethite-solution interface are expected to be >FeO–$Ge(OH)_3^0$ and >FeO–$GeO(OH)_2^-$. This is similar to the model proposed for silica adsorption on goethite (Dietzel, 2002). In this study, we used a traditional 2-pK surface complexation model within the concept of constant capacitance of the electric double layer SCM. Parameters of SCM generated for the goethite—germanic acid—aqueous solution system are listed in Table 1. Intrinsic surface stability constants were obtained by fitting the pH- and [Ge(aq)]-dependence of adsorption for various concentrations of the solid suspension using the MINTEQA2 program. For this purpose, amphoteric acid–base dissociation constants of goethite surface ($pK_1 = 7.3$,

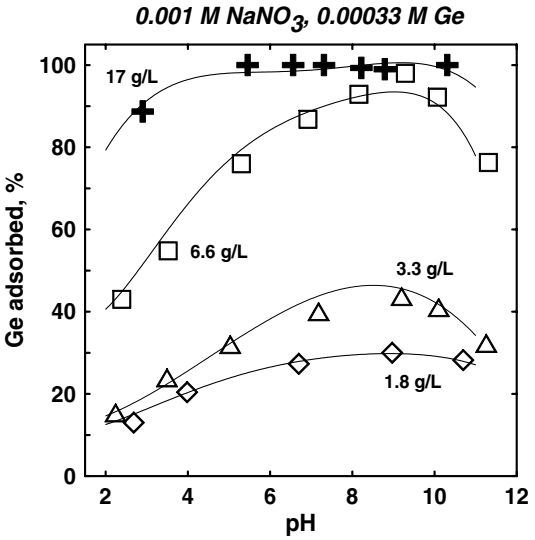

Fig. 3. pH-dependence of Ge adsorption on goethite at various solid/solution ratios. Experimental data are represented by symbols and the fit generated by SCM is shown by solid lines. The numbers at the curves correspond to solid/solution ratio for each series. For the whole range of pH and solid concentration, a unique set of surface complexation constants was found to reproduce experimental results: $\log(>FeO–Ge(OH)_3^0) = 5.3 \pm 0.1$; $\log K(>FeO–GeO(OH)_2^- = -2.7 \pm 0.2$. The error bars are within the size of symbols.

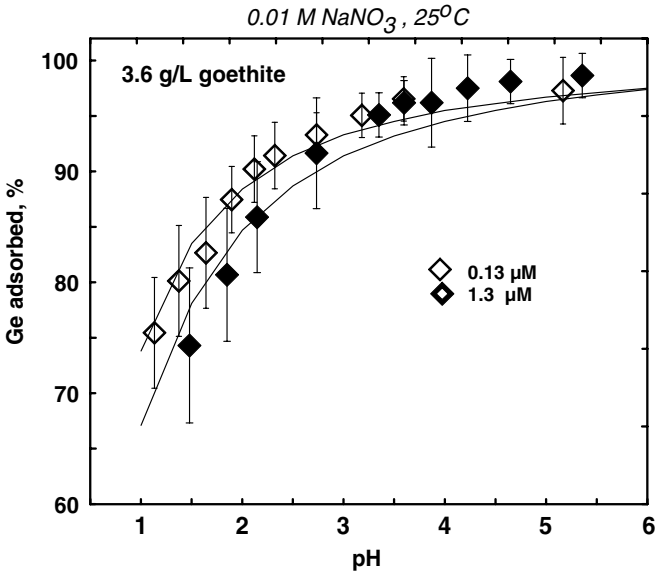

Fig. 4. Ge adsorption on goethite at low solute concentrations: open symbols, $[Ge]_0 = 0.13$ μM; closed symbols, $[Ge]_0 = 1.3$ μM. The set of surface constants ($C = 0.75$ F/m^2): $\log(>FeH_3GeO_4^0 = 5.2$(1.3 μM) and 5.35(0.13 μM) and $\log K(>FeO–GeO(OH)_2^-) = -2.5$(1.3 μM) and -2.8(0.13 μM) used to generate the best fits (solid lines) is consistent, within the uncertainty of proposed model parameters, with the results of the modeling performed at much higher initial Ge concentrations (see Fig. 3).

$pK_2 = 8.9$) were fixed to be same as for hydrous ferric oxide (Dzombak and Morel, 1990), and the capacitance of the electric double layer was kept constant as 0.75 F/m^2 in 0.001 M $NaNO_3$ solution. These values are within the range reported in literature for goethite (cf. Dietzel, 2002). Moreover, maximal Ge surface adsorption density determined in this study allowed to fix the total amount of surface sites available for Ge adsorption as 2.50 ± 0.10 μmol/m^2.

Table 1
Surface complexation model for germanium adsorption on goethite

Surface reaction	$\log K^0_{int}$ (25 °C, $I = 0$)
(1) $>FeOH^0 = >FeO^- + H^+$	−8.9 (fixed)
(2) $>FeOH^0 + H^+ = >FeOH_2^+$	7.3 (fixed)
(3) $Ge(OH)_4 + >FeOH^0 => FeO–Ge(OH)_3^0 + H_2O$	5.3 ± 0.1
(4) $Ge(OH)_4 + >FeOH^0 => FeO–Ge(OH)_2^- + H_2O + H^+$	-2.8 ± 0.15

Surface sites density for Ge adsorption: 2.5 μmol/m^2 (fixed).
Constant capacitance of the EDL: 0.75 F/m^2 (fixed).

Calculated amount of Ge sorbed using SCM parameters of Table 1 are represented as a function of pH and [Ge(aq)] by solid lines in Figs. 2–4. A good agreement is observed between the experimental data and the model. Within the uncertainty of ±0.1 log units, a unique set of surface stability constants reproduces the adsorption equilibria in the wide range of pH and Ge concentrations investigated in the present study. This experimental validation of 2-pK surface complexation model allow the calculation of adsorbed germanium speciation as illustrated in Fig. 5 where the percentage of surface complexes is plotted as a function of pH. For a wide range of goethite concentrations in solution and Ge to surface sites ratio, adsorbed germanium is present in the form of neutral complexes in acid to neutral solutions. At pH > 8, negatively charged complexes become significant and they dominate Ge surface speciation for pH > 10.

Results of germanium adsorption on goethite obtained in the present study can be compared with the abundant

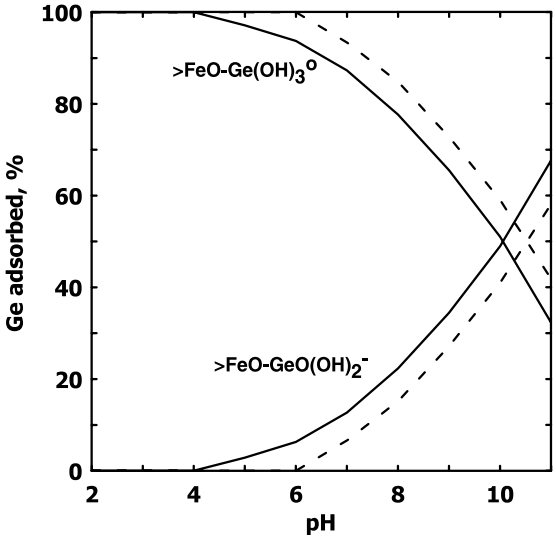

Fig. 5. Speciation of germanium at the goethite—aqueous solution interface at 25 °C, 0.001 M $NaNO_3$, $[Ge]_o = 0.34$ mM. Solid line, 6.6 g/L; dash line, 1.8 g/L of goethite.

data available for (oxy)anions adsorption on goethite and iron hydroxide. Germanium maximal surface sites density (2.5 μmol/m^2) is close to that reported for phosphate (Machesky et al., 1989; Hiemstra and Van Riemsdijk, 1999), arsenate (O'Reilly et al., 2001) and arsenic acid (Grafe et al., 2001), gold(III) chloride $AuCl_4^-$ (Machesky et al., 1991), periodate (Machesky et al., 1989); molybdate (Bibak and Borggaard, 1994; Goldberg et al., 1996), selenate (Rietra et al., 2001), and silica (Davis et al., 2002). The pH-dependent adsorption edge for $Ge(OH)_4$ is similar to that observed for $As(OH)_3$ (Grafe et al., 2001) and $Si(OH)_4$ (Dietzel, 2002). Most of oxyanions are known to adsorb on goethite surface as bidentate binuclear complexes: e.g., arsenate (Harrison and Berkheiser, 1982; Waychunas et al., 1993), molybdate (Bibak and Borggaard, 1994), silica (Vempati and Loeppert, 1989), phosphate and selenite (Hiemstra and Van Riemsdijk, 1999), and sulfate and selenate (Harrison and Berkheiser, 1982). By analogy to these findings, we can suggest that Ge is also adsorbed in the form of binuclear complexes. The 1:1 stoichiometry between Ge(aq) and >FeOH surface sites (Eqs. (1), (2)) is maintained as two metal centers interact with two Ge octahedra at high surface coverages, encountered in most of our adsorption experiments (see Section 3.4.3 below). Note that simple organic acids (lactate, oxalate, malonate, phthalate, and citrate), although also forming bidentate binuclear complexes, exhibit twice lower surface adsorption densities (1.5–1.6 μmol/m^2, Filius et al., 1997). These ligands are unlikely to maintain 1:1 stoichiometry on the surface because their size is much larger than $Ge(OH)_4$(aq) and other inorganic oxyanions.

3.3. Coprecipitation

The list of coprecipitation experiments together with characteristics of produced solid phases is given in Table 2. The rate of Ge coprecipitation with Fe hydroxides, is very fast and similar to the rate of Ge adsorption: stable concentration of incorporated Ge is achieved after ~100 min exposure time depending on solution pH (Fig. 6). At pH 5.7–6.5, the proportion of coprecipitated Ge increases during the first 10–100 min of reaction whereas at pH 4.4, a slight decrease of coprecipitated Ge with time occurs during the first 2–10 min of reaction. The latter can be attributed to very

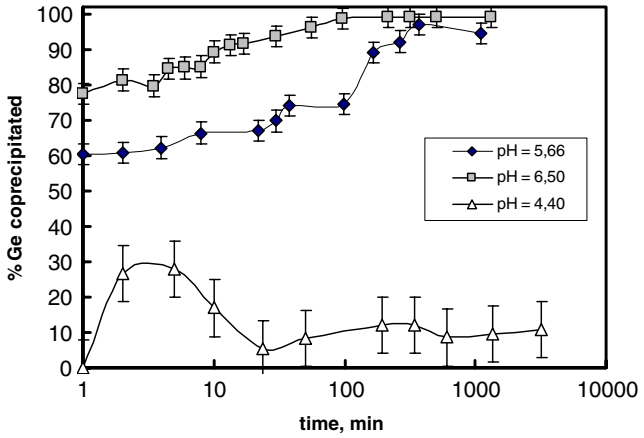

Fig. 6. Kinetics of Ge coprecipitation with iron hydroxide in 0.1 M $NaNO_3$ at 25 °C. Initial conditions: $[Fe]_0 = 3.37$ mM; $[Ge]_0 = 81$ μM. The solid connecting lines are for guiding purposes.

Table 2
List of coprecipitation experiments and solid products formed

Sample	$(Ge/Fe)_0$	$(Ge/Fe)_{solid}$	Fe salt	pH	Time (days)	Solid product
Samples analyzed by EXAFS						
20[a]	0.940	0.936	$FeSO_4$	6.00 ± 0.05	1	Semi-amorphous ferrihydrite
c16	0.31	0.276	$Fe(NO_3)_3$	6.7 ± 0.1	1	Amorphous HFO
5-18	0.20	0.18	$FeSO_4$	10.4 ± 0.1	1	Amorphous HFO
c4-3	0.059	0.056	$FeSO_4$	3.8 ± 0.1	280	Poorly crystalline, ferrihydrite
22	0.078	0.055	$Fe(NO_3)_3$	10.1 ± 0.1	0.06	ND
9-7	0.038	0.037	$FeCl_2$	6.9 ± 0.1	8	Lepidocrocite (well crystalline)
6b-18	0.024	0.024	$FeSO_4$	5.9 ± 0.1	270	ND
6d-17	0.024	0.023	$Fe(NO_3)_3$	8.2 ± 0.1	27	Goethite (well crystalline)
15	0.0094	0.0092	$Fe(NO_3)_3$	6.00 ± 0.05	1	Lepidocrocite
17-ads[b]	0.0094	0.0092	$FeSO_4$	6.00 ± 0.05	1	Lepidocrocite (well crystalline)
16	0.00094	0.0009	$Fe(NO_3)_3$	6.00 ± 0.05	1	Semi-amorphous, goethite & ferrihydrate
14[a]	9.4×10^{-5}	9.2×10^{-5}	$FeSO_4$	6.00 ± 0.05	1	Lepidocrocite (well crystalline)
Samples not analyzed by EXAFS						
C-1-5	0.06 to 0.3	0.02 to 0.2	$FeSO_4$	4.5 ± 0.1	280	Poorly crystalline goethite or ferrihydrite
C-10-15	0.033 to 0.16	0.023 to 0.12	$Fe(NO_3)_3$	8.9 ± 0.5	1	Amorphous HFO
C-17	0.082	0.046	$FeSO_4$	4.6 ± 0.1	1	Amorphous, broad peaks of goethite
6c-13	0.024	0.019	$FeSO_4$	3.9 ± 0.1	270	Goethite (well crystalline)
12[a]	0.0094	0.0091	$FeSO_4$	6.00 ± 0.05	1	Lepidocrocite (well crystalline)
13[a]	0.00094	0.0009	$FeSO_4$	6.0 ± 0.1	1	Lepidocrocite (well crystalline)

Precipitation was performed in 0.1 M $NaNO_3$ (unless indicated) at ambient temperature under light in contact with atmosphere. ND = not determined. HFO = Hydrous ferric oxide.

[a] Background electrolyte is 0.1 M NaCl.

[b] Adsorption of Ge on freshly precipitated $Fe(OH)_3$ obtained by oxidation of $FeSO_4$, Ge-free solution.

slow Fe^{2+} oxidation kinetics at these conditions and the existence of local heterogeneities in supersaturated solutions.

Ge is likely to slow the rate of homogeneous nucleation and subsequent formation of iron hydroxide as noticed in our experiments: the higher the initial (Ge/Fe) ratio, the longer it takes to form the precipitate (not shown). Similar inhibiting effect has been observed for Fe oxides precipitation in the presence of silica, attributed to Si adsorption on nucleus, or silica localization between cluster domains that may inhibit the crystal growth (Schwertman and Thalmann, 1976; Glasauer et al., 1999).

The initial $(Ge/Fe)_{solution}$ ratio exerts the major control on Ge incorporation in the solid. Results of Ge coprecipitation at constant solution pH are presented in Fig. 7 where the $(Ge/Fe)_{solid}$ in the solid is plotted as a function of molar Ge/Fe ratio in the initial solution. Removal of Ge by the precipitation of iron hydroxide is very efficient: the Ge/Fe molar ratio in solid phase achieves 0.50 ± 0.03 corresponding to hydrous iron(III) germanates (Pazenkova, 1967; Bernstein and Waychunas, 1987). The increase of pH favors the incorporation of Ge in the solid as illustrated in Fig. 8 where the molar Ge/Fe ratio in the solid is plotted as a function of solution pH. However, for the pH range of natural waters (from 5 to 10), the effect of pH on Ge coprecipitation is rather weak. This is in agreement with results on Si coprecipitation with ferrihydrite (Schwertman and Thalmann, 1976) and phosphate coprecipitation with iron hydroxide in seawater (Savenko, 1995).

The solid phase formed during iron hydroxide precipitation via Fe^{2+} oxidation or Fe^{3+} hydrolysis and stored 24 h in mother solution is amorphous iron hydroxide containing 12 ± 3 wt% of water. The (Ge/Fe) ratio in precipitated

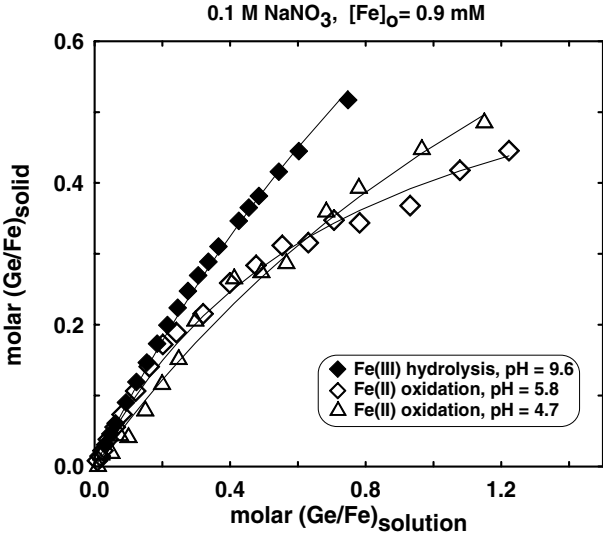

Fig. 7. Ge coprecipitation with Fe oxyhydroxide formed by oxidation of ferrous ion (open symbols) and by hydrolysis of ferric salt (solid diamonds). Exposure time is 24 h. The solid lines represent the fit to the data using semi-empirical Eq. (4) with parameters given in Table 3. The error bars are within the size of symbols.

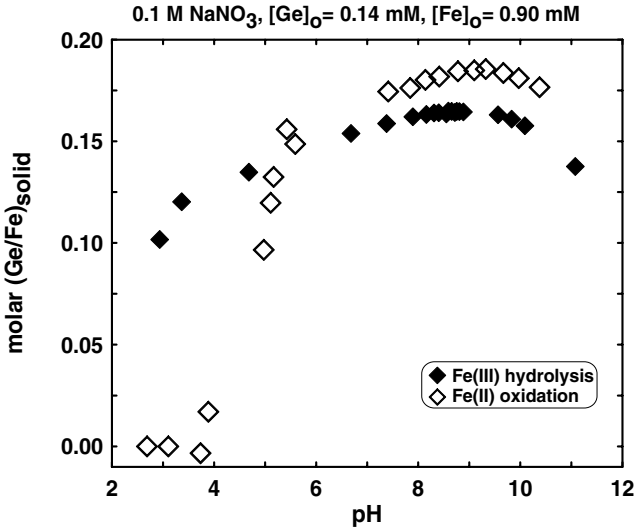

Fig. 8. Ge coprecipitation with Fe oxyhydroxide formed by oxidation of ferrous ion (open diamonds) and by hydrolysis of ferric salt (solid diamonds). Exposure time is 24 h. In the range of natural water conditions ($5 < pH < 10$), pH exerts a weak control on the Ge/Fe ratio in precipitated solid. The error bars are within the size of symbols.

solid exerts the major control on the crystallinity of solid phase: amorphous Fe hydroxide is always formed at $(Ge/Fe)_{solid} > 0.05$. For $0.00012 \leqslant (Ge/Fe)_{solid} \leqslant 0.05$, well crystalline lepidocrocite was identified in our samples that recrystallized into goethite upon aging in mother solution at ambient temperature (Table 2). This is in agreement with previous observations of the silica effect on Fe hydroxide precipitation: Schwertman and Thalmann (1976) observed the increasing proportion of ferrihydrite particles (amorphous ferric oxide) and decreasing proportion of lepidocrocite crystals with increasing Si/Fe in the initial solution; at a Si/Fe ratio of >0.05 no lepidocrocite was formed. The aging of mother solution with solid phase was accompanied by Ge release from coprecipitates and pH decrease by 0.5–0.7 U. $[Ge]_{solution}$ increase by 30–50% was observed during 20–270 h exposure time. Apparently, the growth of lepidocrocite crystallites caused desorption of Ge like in case of As(V) coprecipitation with ferrihydrite (Fuller et al., 1993). In our experiments, the typical time of acquisition of the $(Ge/Fe)_{solid}$ and $(Ge/Fe)_{solution}$ reported in below was 24 h.

The aging of the solution in contact with the precipitated solid phase strongly suggests an irreversible character of the coprecipitation process. Therefore, it cannot be described by thermodynamic equilibrium relationships. A semi-empirical treatment of trace element coprecipitation with iron hydroxide (Savenko, 1999a,b; Savenko and Volkov, 2003) suggests that the atomic ratio of *i* element/Fe in formed solid is proportional to this ratio in the initial solution:

$$(i/Fe)_{solid} = K_d \times (i/Fe)_{solution}, \quad (3)$$

where the partitioning coefficient, K_d, is determined from the linear regression of experimental data obtained at low

(i/Fe) values. At high $(i/\mathrm{Fe})_{\mathrm{solution}}$ values, K_d does not remain constant and a "Langmurian" behavior is observed (Fig. 7). Eq. (3) therefore transforms to:

$$(i/\mathrm{Fe})_{\mathrm{solid}} = K_d \times (i/\mathrm{Fe})_{\mathrm{solution}}/(1 + b \times (i/\mathrm{Fe})_{\mathrm{solution}}), \quad (4)$$

where b is an empirical parameter. The fit of coprecipitation data obtained in this study by Eq. (4) is presented as solid lines in Fig. 7 and the parameters of Eq. (4) are listed in Table 3. The values of K_d determined in this study vary from 0.7 for Fe(II) oxidation process to 1 for Fe(III) hydrolysis. These values can be compared with those from literature data on various oxyanions coprecipitation with iron oxy(hydr)oxides formed by oxidation of ferrous ion in seawater media (pH 6–8, $[Fe^{2+}]_0 = 10$–500 μmol/L): 0.3–0.6 for PO_4^{3-} (Savenko, 1995); 1.0 for $Al(OH)_4^-$ and CrO_4^{3-} (Savenko, 1996, 1999a); 0.7–1.0 for VO_4^{3-} (Savenko, 1998, 1999a); 0.3–0.6 for $H_3BO_3^0$ (Savenko, 2000), and 0.4 for $H_4SiO_4^0$ (Savenko and Volkov, 2003). Schwertman and Thalmann (1976) determined $k_{Si} = 0.8$ in their experiments of silica coprecipitation with Fe hydroxide from highly concentrated solutions at pH 7. It can be seen that the coprecipitation of Ge is comparable with that for other anions and neutral aqueous complexes. Because of the wide range of $(\mathrm{Ge/Fe})_0$ values covered in the present study (i.e., ~1–0.0001), linearly regressed K_d values Eq. (4) can be used for predicting Ge concentration in coprecipitates obtained at lower Ge/Fe ratios as illustrated in Fig. 9. Note that reasonably good agreement between predicted and experimental value is observed for sample #14 having the lowest Ge/Fe ratio $= (9.2 \times 10^{-5})$.

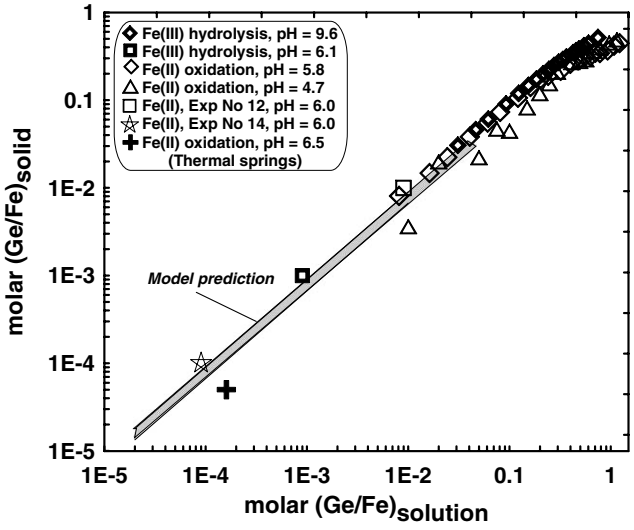

Fig. 9. Molar Ge/Fe ratio in precipitated solid as a function of [Ge]/[Fe] in the initial solution. Experimental exposure time is 24 h. The model prediction using Eq. (3) is shown as shaded area. The cross represents the analysis of a Fe-rich hydrothermal solution of Kamchatka spring (pH 6.5, $[\mathrm{Fe}]_0 = 0.21$ mM) and the massive limonite deposits in equilibrium with this solution, $T = 35$–40 °C (Pokrovsky et al., unpublished results).

3.4. XAFS spectroscopy

3.4.1. Germanic acid aqueous solutions

EXAFS spectra of 0.005 and 0.02 mol/L Ge neutral and basic solutions (Fig. 10) exhibit a first contribution from 4 ± 0.3 oxygens at 1.75–1.76 Å with low thermal/structural disorder ($\sigma^2 \sim 0.002$ Å^2) (Table 4). These parameters are similar to those reported for tetrahedral GeO_2 having a quartz-like structure and for numerous germanates (e.g., Nishi and Takéuchi, 1992; Yoshiasa et al., 1999). Note that XANES spectra of the studied solutions and solids (not shown) are also very similar in shape and edge-energy position (~11108 ± 0.5 eV, taken at the maximum of the first derivative of the spectrum). This strongly suggests a tetrahedral environment for Ge in aqueous solution in a wide pH range consistent with the formation of germanic acid or its dissociation products. The Ge–O distance and σ^2 are slightly higher in basic conditions than at neutral pH (Table 4), suggesting a slight distortion of the GeO_4 tetrahedron in basic conditions. This is consistent with previous solubility, potentiometric and Raman spectroscopy studies showing that Ge aqueous speciation is dominated by the neutral $Ge(OH)_4$ complex at pH < 9 and by the negative $GeO(OH)_3^-$ species at higher pH (Baes and Mesmer, 1976; Pokrovski and Schott, 1998a).

A weak but persistent 2nd shell contribution apparent on the FT spectra at ~2.5 Å (Fig. 10) is likely to arise from multiple scattering events within the symmetrical GeO_4 tetrahedron. This was confirmed by FEFF calculations carried out on $[GeO_4(\pm H_4) \pm (H_2O)_n]$ clusters which show that MS paths within the GeO_4 cluster such as a triangular path Ge–O1–O2–Ge ($R_{ms} = 3.19$ Å, degeneracy = 12), an angular path Ge–O1–Ge–O2 ($R_{ms} = 3.51$ Å, degeneracy = 12), and a linear path Ge–O1–Ge–O1 ($R_{ms} = 3.51$ Å, degeneracy = 4) may contribute to the EXAFS signal and likely form to the apparent 2nd shell contribution. Their DW factors were estimated using the equation-of-motion (EM) and recursion method (RM) models incorporated in the FEFF 8 code (Poiarkova, 1999; Poiarkova and Rehr, 1999). Both models yielded similar σ^2 values of 0.005 ± 0.002 Å^2 for the three MS paths at ambient temperature. It can be seen in Fig. 10 that the consideration of these MS paths in the fit reasonably accounts for the

Table 3
Parameters of Eq. (4) for coprecipitation experiments performed in 0.1 M $NaNO_3$ at 25 °C

Process	pH	$[\mathrm{Fe}]_0$ (μmol/L)	$[\mathrm{Ge}]_0$ (μmol/L)	K_d	b
Fe(II) oxidation	4.7 ± 0.3	860	8.3–960	0.67 ± 0.02	0.48 ± 0.02
Fe(II) oxidation	5.8 ± 0.3	930	8.3–1240	0.90 ± 0.02	1.30 ± 0.05
Fe(III) hydrolysis	9.56 ± 0.02	895	28–700	0.975 ± 0.025	0.50 ± 0.02

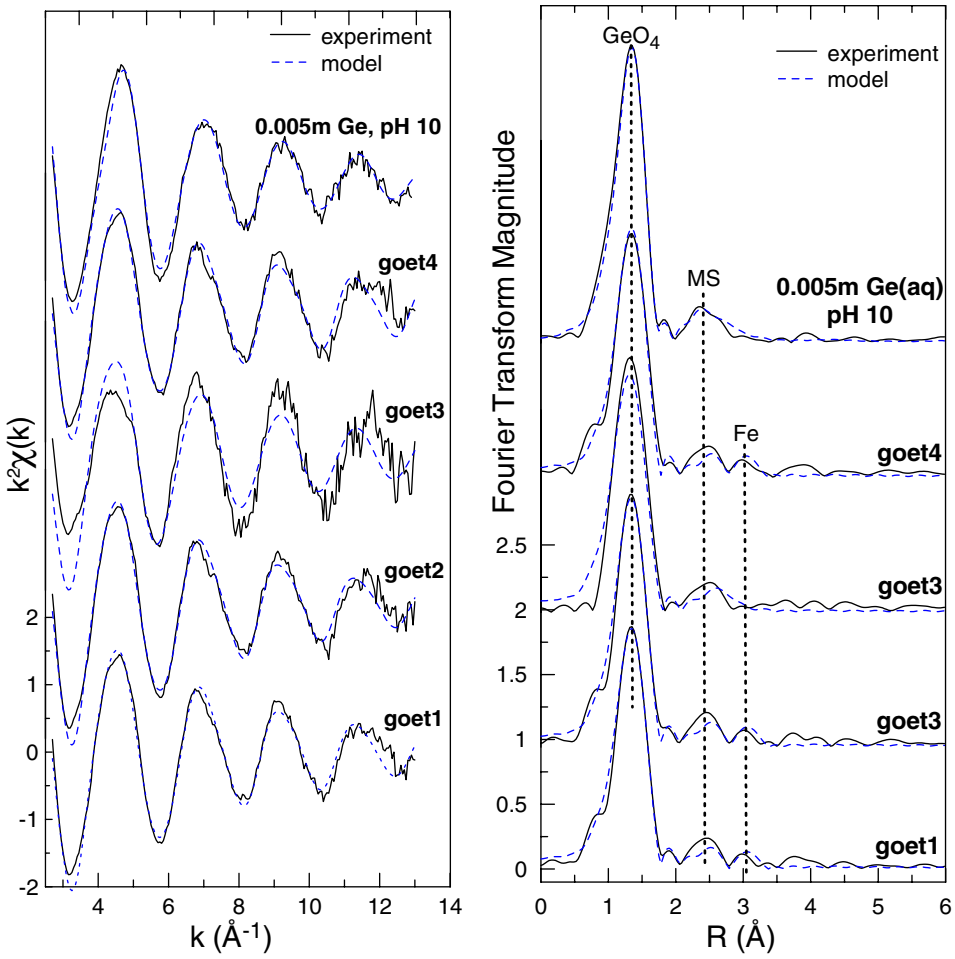

Fig. 10. k^2-weighted EXAFS spectra at Ge *K*-edge and their Fourier Transforms (not corrected for phase shift) of aqueous and sorbed Ge samples (see Table 4 for sample description). Vertical dashed lines indicate the positions of the first atomic shell around Ge composed of four oxygens (labeled GeO_4), multiple scattering (labeled MS) within the GeO_4 tetrahedron, and a second shell of iron atoms (labeled Fe).

Table 4
Structural parameters of the atomic environment of germanium in aqueous solution and adsorbed on goethite surface at ambient temperature and pressure

Sample	E^0 (eV)	atom	N (atoms)	R (Å)	σ^2 (Å^2)	Δe (eV)	R-factor
Aqueous Ge							
0.02 m Ge, pH 4.5 ge1	11107.6	O	4.1 ± 0.2	1.751 ± 0.005	0.0020	7.0	0.007
0.02 m Ge, pH 11.7 ge4	11107.6	O	4.1 ± 0.2	1.762 ± 0.005	0.0030	8.0	0.010
0.005 m Ge, pH 10.0 geaq00	11107.6	O	4.3 ± 0.3	1.759 ± 0.008	0.0028	7.2	0.009
Adsorded Ge							
1.8 g/L FeOOH, pH 7.6	11107.7	O	4.0 ± 0.5	1.76 ± 0.01	0.0020	6.0	0.013
$[Ge]_{surf}$ = 2.5 μmol/m^2 goet1		Fe	0.7 ± 0.3	3.3 ± 0.1	0.006		
6.0 g/L, pH 7.4	11107.9	O	4.3 ± 0.6	1.76 ± 0.01	0.0022	6.0	0.013
$[Ge]_{surf}$ = 2.5 μmol/m^2 goet2		Fe	0.8 ± 0.4	3.3 ± 0.1	0.007		
6.6 g/L, pH 2.2	11107.9	O	4.2 ± 0.5	1.76 ± 0.02	0.002	5.0	0.05
$[Ge]_{surf}$ = 2.5 μmol/m^2 goet3							
6.6 g/L, pH 11.0	11107.9	O	3.8 ± 0.6	1.76 ± 0.01	0.002	6.0	0.01
$[Ge]_{surf}$ = 2.5 μmol/m^2 goet4		Fe	0.8 ± 0.4	3.3 ± 0.1	0.005		
Error of EXAFS fit	± 0.5 eV				±30%	±2 eV	

Atom = nature of scattering atom; R = germanium-scatterrer mean distance, N = scatterrer coordination number; E^0 = energy of the maximum of 1st derivative of the spectrum; σ^2 = squared Debye-Waller factor (DW, relative to $\sigma^2 = 0$ adopted in the calculation of reference amplitude and phase functions by FEFF8, see text); Δe = difference between experimental energy and that estimated by FEFF; R-factor defines goodness of the total fit in R-space as described in FEFFIT (Newville, 2001). For all samples the fitted k-range and R-range were 3.5–11.0 Å^{-1} and 1.1–3.5 Å, respectively. The following multiple scattering paths arising from the GeO_4 tetrahedron as calculated using FEFF8 (see text) were included in all fits: triangular Ge–O1–O2 ($R_{ms} = 1.82 \times R_{O1}$, degeneracy=12); angular Ge–O1–Ge–O2 ($R_{ms} = 2 \times R_{O1}$, degeneracy = 12); and linear Ge–O1–Ge–O2 ($R_{ms} = 2 \times R_{O1}$, degeneracy = 4); their DW factors were assumed to be triple of the corresponding values for the 1st Ge shell (see text).

2nd shell contribution observed in Ge aqueous solutions. Possible contributions of hydrogen atoms ($R_{Ge-H} \sim 2.7$ Å) from OH-groups of the $Ge(OH)_4$ complex were also tested. Although their consideration improves somewhat the fit quality, the derived amplitudes and σ^2 exhibit large errors and are sensitive to the fitted k-range. This poor fit robustness is likely due to the very weak backscattering signal from the light hydrogen atoms. Although consideration of oxygen atoms from water molecules of the outer-sphere hydration shell also yields statistically better fits in comparison to the MS model, the R_{Ge-OH_2} distance found (2.8 ± 0.1 Å) is too short for a water molecule linked to the $Ge(OH)_4$ or $GeO(OH)_3^-$ via hydrogen bonds. By analogy with aqueous silicic acid (Rustad and Hay, 1995), a diffuse and disordered hydration shell is expected at ~4 Å around Ge. Moreover, the strong similarity of the 2nd shell amplitude and phase structure in germanic acid aqueous solutions at temperatures from 20 to 450 °C (Pokrovski et al., 2005) strongly favors the MS hypothesis versus outer-sphere hydration shell. Thus, only the MS paths discussed above were considered; they were also included in fits of Ge adsorption and co-precipitation samples.

3.4.2. Germanium adsorbed on goethite

XANES spectra of adsorbed Ge (not shown) exhibit shapes and edge-energy positions (~11,108 ± 1 eV) very close to those of aqueous germanic acid, suggesting a similar tetrahedral environment for Ge in its complexes on goethite surface. As for the aqueous samples, the 1st Ge shell is composed of four oxygens at an average distance of 1.76 ± 0.01 Å. Attempts to include a Ge–O contribution with a longer distance (~1.9 Å), which could correspond to an octahedral structure GeO_6 as in rutile-like GeO_2 and stottite, $FeGe(OH)_6$ (Baur and Khan, 1971; Ross et al., 1988), failed: fits always converged to a single shell with $R_{Ge-O} = 1.76$ Å and $N_{Ge-O} = 4.0 \pm 0.2$. Thus, within the limit of the spectral resolution, the octahedral Ge, if present, cannot account for more than 5–10% of total adsorbed Ge.

The four goethite samples investigated exhibit similar weak second-shell features in the range of 2.0–3.5 Å (not corrected for phase shift, Fig. 10). Their phase and amplitude are close to those for aqueous Ge thus suggesting the dominance of the MS events from GeO_4 cluster (see previous section). Another extremely weak signal is apparent at ~3 Å for three samples. Both spectra examination at different k-weightings and qualitative wavelet transforms (Munoz et al., 2003) suggest the presence of heavy backscatterers like Fe or Ge. Following these observations, this contribution was tentatively fitted using about 0.5–1 Fe atom at 3.3 ± 0.1 Å (Table 4). This distance may correspond to double-corner bi-dentate (C_2-type) complexes between the Ge-tetrahedron and two adjacent Fe-octahedra sharing a common edge at the goethite surface. Such a structure is similar to those formed by analogous oxy-acids and their anions with iron and aluminum hydroxide surfaces (H_4SiO_4, Pokrovski et al., 2003; AsO_4^{3-} and SeO_4^{2-}, Waychunas et al., 1993; Manceau and Charlet, 1994; H_3AsO_3, Manning et al., 1998; CrO_4^{2-}, Fendorf et al., 1997). However, it should be kept in mind that the average nature of an EXAFS signal and its high sensitivity to disorder typical for adsorption processes, together with mediocre signal/noise ratio of our adsorption samples (exploitable k-range is between 3 and 11 $Å^{-1}$) do not allow definitive conclusion about the existence of other types of surface complexes. Germanium atomic environment may be multiple, particularly at the high surface coverage investigated in this study, with different complexes simultaneously present at the FeOOH surface. Moreover, the C_2-complexes might have different tilt angles so that EXAFS 'sees' an average distance and number of neighbors of such complexes and the resulting total amplitude may be lowered by destructive interferences from different geometries.

3.4.3. Germanium co-precipitated with Fe(III) oxyhydroxides

XANES spectra of the majority of co-precipitated samples (not shown) exhibit shapes and energy positions (energy of the edge 1st derivative, E^0, is ~11,107 ± 1 eV, Table 5) which are close to those for aqueous germanic acid, suggesting the dominant presence of a tetrahedral environment around Ge co-precipitated with ferric iron hydroxides. The only exception is sample #14 (Table 2) having the lowest Ge/Fe molar ratio ($Ge/Fe = 9.2 \times 10^{-5}$). Its XANES spectrum is different from the others and exhibits a higher edge energy ($E° \sim 11{,}109.3 \pm 0.5$ eV). This value is close to that for the rutile-type GeO_2 in which Ge is hexa-coordinated with oxygen (Baur and Khan, 1971), thus suggesting a part of Ge being in coordination 6 in sample #14. This is confirmed quantitatively by EXAFS spectra analysis.

EXAFS spectra of selected representative samples from co-precipitation experiments are shown in Fig. 11. Analysis of the first shell revealed two distinct types of Ge atomic environment (see Table 5). All samples with high Ge/Fe ratios ($Ge/Fe \geqslant 0.1$: #20, c16, 5-18), and those separated from the solution after a short period of time (<1 day) having intermediate Ge/Fe (~0.01: #15, 17-ads) show 4 ± 0.3 oxygen atoms at 1.76 ± 0.01 Å around Ge, with low σ^2, very close to those in germanic acid aqueous solutions and quartz-like GeO_2 ($\sigma^2 \sim 0.0025$ $Å^2$). The Ge–O distance found is typical of those reported for various low-temperature alkaline and alkaline-earth metal germanates and high-temperature iron germanates—silicate analogs ($R_{Ge-O4} = 1.74$–1.76 Å, e.g., Nishi and Takéuchi, 1992; Barbier and Lévy, 1998). No influence of pH or the nature of Fe salt (ferric versus ferrous iron nitrate, chloride or sulfate) used in the co-precipitation experiments was observed. The presence of 6-coordinated Ge was not detected indicating that the number of oxygens linked to $^{[6]}$Ge would not exceed 0.1–0.2 atom which might correspond to 2–5% of the total Ge in these samples.

Table 5
Structural parameters of the first atomic shell of germanium co-precipitated with Fe(III) oxy-hydroxides

Sample	T (K)	Ge/Fe	k-range (A^{-1})	E^0 (eV)	Atom	N (atoms)	R (Å)	σ^2 ($Å^2$)	Δe (eV)
20	293	0.936	3.2–12.9	11107.6	O	4.4 ± 0.4	1.76 ± 0.01	0.0029	6.0
c16	293	0.276	2.8–13.0	11106.3	O	3.9 ± 0.3	1.76 ± 0.01	0.0023	8.0
5-18	293	0.18	2.8–12.2	11106.8	O	4.2 ± 0.3	1.77 ± 0.01	0.0030	8.0
15	11	0.0092	2.9–11.8	11107.6	O	4.2 ± 0.3	1.77 ± 0.01	0.0027	7.7
17-ads	11	0.0092	2.9–12.2	11107.6	O	4.1 ± 0.3	1.77 ± 0.01	0.0021	7.9
c4-3	293	0.056	2.8–13.0	11106.8	O1	3.1 ± 0.5	1.78 ± 0.01	0.0030	8.0
					O2	0.7 ± 0.2	1.92 ± 0.02	0.0030	
6d-17	293	0.023	2.8–13.0	11107.6	O1	3.2 ± 0.4	1.77 ± 0.01	0.0025	7.5
					O2	0.7 ± 0.2	1.91 ± 0.04	0.0030	
6b-18	11	0.024	2.8–12.9	11107.4	O1	3.4 ± 0.3	1.78 ± 0.01	0.0020	8.5
					O2	0.8 ± 0.2	1.92 ± 0.03	0.0020	
	293		2.8–12.9	11107.4	O1	3.5 ± 0.2	1.77 ± 0.01	0.0020	8.5
					O2	0.7 ± 0.2	1.92 ± 0.03	0.0020	
16	11	0.0009	3.8-12.3	11107.3	O1	3.1 ± 0.4	1.76 ± 0.01	0.0016	7.4
					O2	1.1 ± 0.3	1.90 ± 0.03	0.0020	
9-7	11	0.037	3.8-11.9	11107.3	O1	3.0 ± 0.3	1.79 ± 0.02	0.0020	9.5
					O2	1.3 ± 0.3	1.95 ± 0.05	0.0020	
	293		3.8–11.9	11107.7	O1	3.1 ± 0.7	1.79 ± 0.01	0.0020	9.8
					O2	1.3 ± 0.3	1.94 ± 0.05	0.0020	
14	11	0.000092	3.7–11.5	11109.3	O1	3.5 ± 1.0	1.79 ± 0.01	0.0030	9.2
					O2	2.0 ± 0.5	1.94 ± 0.05	0.0030	
Error				±0.5 eV				±30%	±1.5 eV

T (K) = temperature of measurement in Kelvin; Ge/Fe = germanium-to-iron molar ratio in the precipitate; see Table 2 for other sample characteristics, and Table 4 for explanation of EXAFS parameters. All fits were processed in the R-range between 1.1 and 3.4–3.7 Å; fit quality is reported in Table 6.

In contrast to the Ge high-concentration coprecipitates, samples with low Ge/Fe ratios (<0.001: #16) and those with intermediate ratios ($0.01 < Ge/Fe < 0.1$) but having longer ageing times (>8 days: #c-3-4, 6d-17, 6b-18, 9-7) exhibit a splitting of the 1st atomic shell with Ge in both tetrahedral ($R = 1.77 \pm 0.02$ Å, $N = 3.0$–3.5) and octahedral (R=1.92 ± 0.03 Å, $N = 0.5$–1.3) coordination with oxygen (Table 5). The octahedral contribution becomes more pronounced at the lowest Ge/Fe (0.00012, #14) with $N_{Ge\text{–}O6} = 2.0 \pm 0.5$ atoms which represents at least ~30% of the total Ge in this sample, and is in agreement with the XANES spectra (see above). No difference within error in structural parameters and degree of disorder (DW factors) both for first and next-nearest shells were observed for same samples measured in a cryostat (11 K) and at ambient conditions (e.g., #6b-18, 9-7). This demonstrates that most of disorder associated with the germanium environment in co-precipitated samples is structural, and that thermal motion has no detectable effect on the spectra.

All samples exhibit next-nearest atomic shells composed mostly of heavy atoms (likely Fe and/or Ge) with amplitudes generally decreasing with increasing Ge/Fe ratios (Fig. 11). This likely reflects the increase of disorder at high Ge/Fe ratios and the increased number of possible geometries attenuating the total signal. Modeling of the second-shell features (Table 6) suggests three types of atomic environment around Ge. For the most concentrated sample (#20, Ge/Fe = 1.22) exhibiting very low 2nd shell amplitudes, only a single Fe/Ge contribution at ~3.3 Å could be detected. The atomic numbers of Fe and Ge differ only by 6, making their backscattering waves similar. This precludes unambiguous distinction between Ge–Fe and Ge–Ge pairs by EXAFS in our samples having high Ge contents. The Ge-(Ge/Fe) distance found in the most concentrated sample (#20) is, however, different from the typical Ge–Ge distances in GeO_2 oxides (2.9 and 3.4 Å in quartz-like GeO_2, and 3.1 and 4.4 Å in rutile-like GeO_2; Jorgensen, 1978; Baur and Khan, 1971), and in chain-like iron germanates (typically ~3.0–3.2 Å between two GeO_4 tetrahedra sharing a common summit, e.g., Barbier and Lévy, 1998). This suggests that Fe is a more preferable candidate for the next-nearest shell of our samples, and neither germanium oxides nor polymeric germanates formation occurs during the co-precipitation.

Thus, all other less concentrated samples, having more pronounced next-nearest shells than sample #20, were modeled with two or three Fe subshells and including the MS paths within GeO_4 cluster as discussed above. During the fitting procedure, care was taken to insure that the number of variables in the fit (R, N, and σ for each subshell (O1 ± O2 in the 1st shell, Fe1 + Fe2 ± Fe3 in the 2nd shells and a common Δe value) was less than the number of statistically independent points ($N_{idp} = 2\Delta k \Delta R/\pi$, which typically ranged from 11 to 16 for our spectra depending on the exploitable k-range). Following this restriction, and in order to avoid high correlations between N and σ values, the DW parameters for all Fe subshells were assumed identical. The best-fit σ^2 values found (0.005–0.01 $Å^2$) are similar to those reported for arsenate and arsenite co-precipitated with iron hydroxides and sulfides (Waychunas et al., 1993; Farquhar et al., 2002). However, because of the limitations above, we estimate the uncertainty on the σ^2 for Ge–Fe paths as about ±30% of the value which yields a similar error in the determination of

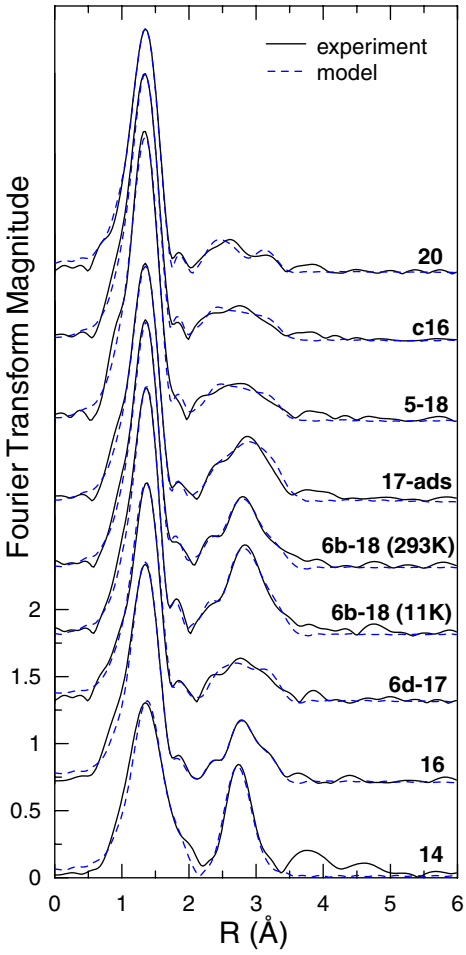

Fig. 11. k^2-weighted EXAFS spectra at Ge *K*-edge and their Fourier Transforms (not corrected for phase shift) of co-precipitated Ge–Fe samples (see Table 2 for sample description).

Table 6
Structural parameters of the next-nearest atomic shells around Ge(IV) co-precipitated with Fe(III) oxy-hydroxides

Sample	*T* (K)	Ge/Fe	Atom	*N* (atoms)	*R* (Å)	σ^2 (Å^2)	*R*-factor
20	293	0.936	Fe	0.8 ± 0.4	3.36 ± 0.03	0.008	0.0080
C16	293	0.276	Fe1	0.7 ± 0.3	2.87 ± 0.04	0.010	0.0038
			Fe2	2.0 ± 0.5	3.38 ± 0.02	0.010	
5–18	293	0.18	Fe1	0.6 ± 0.4	2.87 ± 0.05	0.009	0.0078
			Fe2	2.1 ± 0.6	3.39 ± 0.03	0.009	
15	11	0.0092	Fe1	0.8 ± 0.4	2.82 ± 0.06	0.006	0.0060
			Fe2	1.0 ± 0.5	2.99 ± 0.03	0.006	
			Fe3	2.9 ± 0.6	3.39 ± 0.02	0.006	
17-ads	11	0.0092	Fe1	1.1 ± 0.6	2.93 ± 0.06	0.009	0.0070
			Fe2	3.0 ± 1.5	3.40 ± 0.02	0.009	
c-4-3	293	0.056	Fe1	1.1 ± 0.6	2.82 ± 0.06	0.01	0.0061
			Fe2	2.0 ± 1.0	3.01 ± 0.04	0.01	
			Fe3	2.6 ± 1.3	3.42 ± 0.02	0.01	
6d-17	293	0.023	Fe1	0.5 ± 0.3	2.90 ± 0.04	0.008	0.0045
			Fe2	2.0 ± 0.5	3.40 ± 0.03	0.008	
6b-18	11	0.024	Fe1	1.0 ± 0.5	2.81 ± 0.05	0.007	0.0058
			Fe2	2.2 ± 1.0	3.01 ± 0.03	0.007	
			Fe3	3.0 ± 0.5	3.43 ± 0.02	0.007	
	293		Fe1	1.0 ± 0.8	2.81 ± 0.05	0.008	0.0059
			Fe2	1.7 ± 1.0	3.01 ± 0.03	0.008	
			Fe3	2.5 ± 0.5	3.42 ± 0.02	0.008	
16	11	0.0009	Fe1	1.1 ± 0.7	2.84 ± 0.05	0.008	0.0031
			Fe2	2.4 ± 1.0	3.05 ± 0.03	0.008	
			Fe3	2.3 ± 0.8	3.38 ± 0.03	0.008	
9-7	11	0.037	Fe1	1.4 ± 0.5	3.05 ± 0.04	0.006	0.0076
			Fe2	1.1 ± 0.5	3.42 ± 0.04	0.006	
	293		Fe1	1.0 ± 0.3	3.05 ± 0.03	0.006	0.0080
			Fe2	0.9 ± 0.4	3.41 ± 0.04	0.006	
14	11	0.000092	Fe1	1.1 ± 0.9	2.85 ± 0.10	0.006	0.016
			Fe2	4.0 ± 1.0	3.06 ± 0.03	0.006	
Error						±30–50%	

See Tables 4 and 5 for explanation of EXAFS parameters. *R*-factor corresponds to the total fit (first plus next-nearest shells) in *R*-space. DW factors of all Fe sub-shells were assumed identical (see text).

Ge–Fe coordination numbers. No other lighter scatterers like SO_4/Cl/NO_3 anions or H_2O trapped during co-precipitation were found to match satisfactorily the experimental spectra or yielded unphysical values (e.g., negative to nil σ^2, high (>5–10) number of neighbors). Moreover, the presence of oxygens above ~3.2 Å from the FeO_6 octahedra framework, ubiquitous in ferric-iron hydroxide structures, could not be detected. This may be explained by the high degree of disorder associated with these light scatterers and the predominance in the signal of heavy Fe neighbors beyond 3 Å.

The samples with $0.01 \leqslant Ge/Fe \leqslant 0.4$ and most Ge in tetrahedral coordination (i.e., >80%) were represented by amorphous solids or very poorly crystalline goethite (Table 2). For these samples, the best models were obtained with two or three iron contributions at ~2.8, 3.0, and 3.4 Å (Table 6). The last Ge–Fe distance likely corresponds to double-corner bi-dentate (C_2-type) complexes between the Ge-tetrahedron and Fe-octahedra of iron hydroxide with a tilt angle close to zero. Similar anion-Fe distances were found for arsenite, arsenate and selenate adsorbed onto or co-precipitated with Fe hydroxides (Waychunas et al., 1993; Manceau and Charlet, 1994; Manning et al., 1998; Farquhar et al., 2002). The shortest Ge–Fe distance (2.8 Å) may correspond to edge-sharing complexes between GeO_4 and FeO_6 (E_2-type) and is also close to those reported for As, Cr, and Se on Fe hydroxides (2.6–2.8 Å; e.g., Manceau and Charlet, 1994; Manceau, 1995 and references therein). Note that the length of the edge of the regular Ge-tetrahedron ($R_{Ge-O} = 1.75$ Å) and Fe-octahedron ($R_{Fe-O6} = 2.00$ Å) are very similar (~2.86 Å), which should favor this kind of bonding with minimal distortion. Geometric considerations show that the intermediate Ge–Fe distance detected in some samples (3.0 Å) is too long for an edge-sharing linkage. The 3-Å Ge–Fe contribution is likely to arise from another type of C_2 complex with an elevated tilt angle between GeO_4 and two adjacent Fe octahedra (Fig. 12). Moreover, for samples with octahedral Ge accounting for up to 20% as inferred from the 1st shell analysis, [6]Ge substituting for Fe in octahedral positions may also contribute to the EXAFS signal arising from the Fe subshells at 3.0 and 3.4 Å. Because

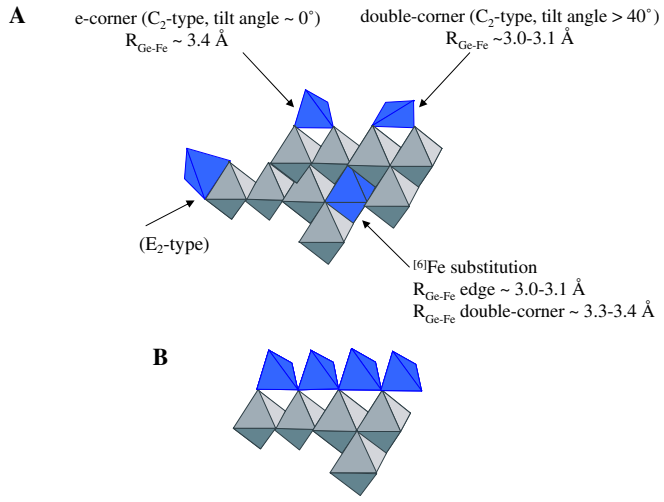

Fig. 12. (A) Schematic structures of the atomic environment of Ge(IV) adsorbed onto or co-precipitated with Fe(III) oxy-hydroxides. Light-grey octahedra denote the $Fe(O/OH)_6$ coordination sphere with the metal in the centre; dark-grey tetrahedra and octahedra stand for Ge(IV) four- and six-coordinated with O/OH, respectively. (B) Bidentate binuclear adsorbed complexes that maintain 1:1 stoichiometry between Fe surface centers and $Ge(OH)_4$ according to reactions (1) and (2).

the structure of both Fe(III) amorphous oxy-hydroxide and crystalline minerals consists of distorted $Fe(O/OH)_6$ octahedra sharing a common edge with $R_{Fe-Fe} \sim 3.0 \pm 0.05$ Å and a double corner with $R_{Fe-Fe} \sim 3.4 \pm 0.1$ Å (e.g., Manceau and Combes, 1988), Ge substituting for Fe in an octahedron will "see" the neighboring edge- and corner-sharing FeO_6 at similar distances. Assuming typical numbers of 4 and 2, respectively, for Fe edge and corner neighbors around an iron atom, which is typical of those found at the late stages of Fe hydrolysis and in $FeO_y(OH)_x$ precipitates (Combes et al., 1989), the number of iron neighbors in the EXAFS signal from $^{[6]}$Ge is 0.6 and 0.3 atoms for edge and corner linkages, respectively, for samples in which about 15% of Ge was found in the octahedral coordination (e.g., #6b-18, 16, 9-7). The rest of Ge is in tetrahedra forming binuclear C_2-type complexes with FeO_6, which corresponds to $0.85 \times 2 = 1.7$ atoms of Fe (if two corners of $[GeO_4]$ are bound) and 3 atoms of Fe (if all four corners are bound) "seen" by Ge in each complex. Thus, because of the 'average' nature of the EXAFS signal, the overall number of iron atoms seen by Ge can exceed 2 for both types of linkages. It is in agreement with the values between 2 and 3 found in several samples for the Fe coordination numbers at 3.0 and 3.4 Å.

The most dilute sample, corresponding to lepidocrocite and containing at least 30% of 6-coordinated Ge (#14, Ge/Fe 0.00012, Tables 2 and 6) exhibits a different second-shell structure with a dominant contribution from 4 ± 1 iron atoms at 3.06 Å (Fig. 13). This distance is higher than that found in more concentrated amorphous samples (2.99–3.01 Å, e.g., #6b-18, c4-3, 15) and exactly matches the distance between two edge-sharing iron octahedra in lepidocrocite structure ($R_{Fe-Fe} = 3.06$–3.08 Å, $N_{Fe-Fe} = 6$; Wyckoff, 1963). This demonstrates that roughly half of

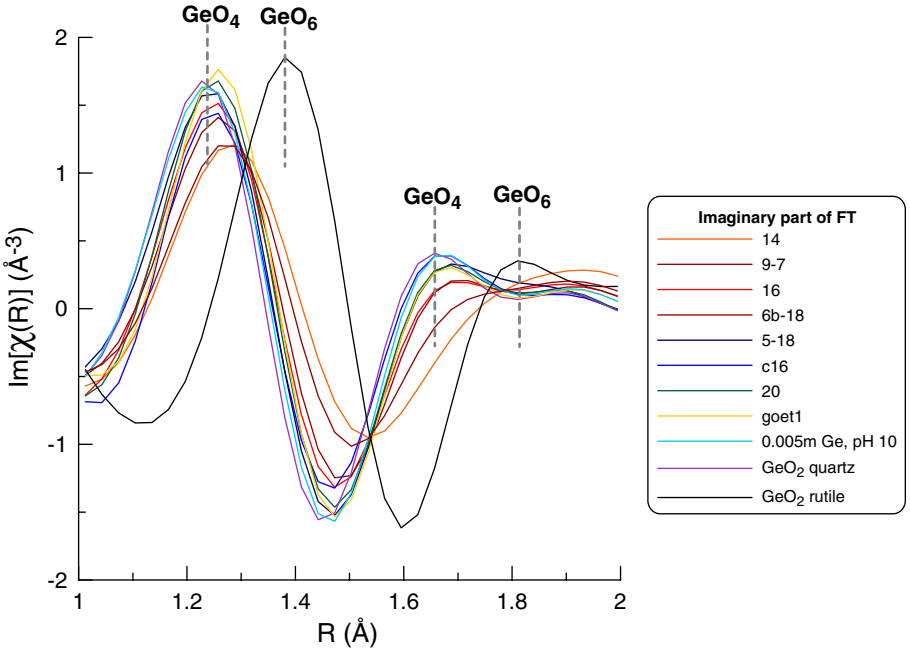

Fig. 13. Imaginary part of the Fourier Transform (not corrected for phase-shift) of the Ge first atomic shell of selected adsorption and co-precipitation samples and solid references. Vertical dashed lines indicate the features corresponding to tetrahedral and octahedral Ge coordination. It can be seen that for adsorbed and co-precipitated samples with high Ge/Fe ratios, these features closely match those of aqueous germanic acid and quartz-like germanium dioxide, suggesting the dominant tetrahedral coordination. In contrast, for low Ge/Fe ratios and/or long reaction times (samples #6b-18, 16, 9-7, 14), there is a detectable contribution from octahedral Ge which induces shifts in the shape and position of main maxima towards those characteristic of rutile-like germanium dioxide. The presence of 6-coordinated Ge in these samples is quantitatively confirmed by EXAFS modeling (see Table 5).

Ge substitutes for Fe, in good agreement with the 1st shell parameters. The rest of Ge is in tetrahedral coordination and it is likely linked to Fe octahedra via a common edge, with a Ge–Fe distance of ~2.8 Å (Table 6). Following the great sensitivity of EXAFS to disorder which leads to large uncertainties associated with coordination numbers, it is difficult to define the exact status of the tetra-coordinated Ge in this sample.

Overall, the XAFS results demonstrate essentially a tetrahedral coordination for germanium in iron hydroxide compounds obtained in our co-precipitation experiments. The largest changes in Ge chemical status between solution and solid phase occur for the lowest Ge/Fe ratios in the fluid and longest reaction times, conditions closer to those of natural samples. This is consistent with results of Bernstein and Waychunas (1987) who reported, using XAFS, the occurrence of octahedrally coordinated Ge ($R_{Ge-O} = 1.88$ Å) substituting for Fe(III) in Ge-rich goethite and hematite from the weathering zone of the copper-arsenic sulfide Apex Mine (Utah, USA). These samples contain up to 1 wt% of Ge which roughly corresponds to Ge/Fe ratios of 0.01. Our co-precipitated samples of lepidocrocite and ferrihydrite exhibiting similar Ge/Fe ratios show, however, only small proportion of Ge (<10–20%) in octahedral coordination. The substitution of Ge for Fe(III) in natural samples is facilitated both by a much slower kinetics of formation of iron-hydroxide than those in laboratory experiments, longer aging times and by the presence in natural environments of other cations like Fe(II), Ca(II), Pb(II) which may favor the substitution of Ge(IV) for Fe(III) through a charge-compensation mechanism like Ge(IV) + Me(II) = 2Fe(III).

4. Applications for Ge versus Si fractionation in natural settings

A quantitative comparison between Ge and Si is not possible due to different model parameters for adsorption (i.e., diffuse double layer model in Dietzel, 2002 versus constant capacitance model in this study) and experimental conditions of coprecipitation (i.e., seawater in Savenko and Volkov (2003) versus 0.1 mol/L $NaCl/NaNO_3$ solutions in this study). However, preliminary analyses demonstrates that Ge is likely to be adsorbed more efficiently by Fe hydroxide surfaces since $\log K_{3,4}$ are higher for Ge (Table 1) compared to silica (Dietzel, 2002) and that the maximal adsorption density on goethite at pH 7–8 is higher for Ge (2.5 ± 0.1 μmol/m^2) compared to silica (2.2 ± 0.1 μmol/m^2, Dietzel, 2002). Furthermore, one can calculate at the same pH value the empirical partitioning coefficient between adsorbed and aqueous Ge or Si (K_{ads}) defined as [m(Ge,Si)$_{ads}$/surface area(solid)]/[m(Ge,Si)$_{aq}$/m(solution)]. At pH about 7–7.2, we found for Ge (Fig. 2a) $K_{ads} = 0.0096$ L/m^2 whereas for Si (Table 2, Dietzel, 2002) the $K_{ads} = 0.0083$ L/m^2.

Ge is also more effectively co-precipitated with iron hydroxide than Si: K_d for Ge in neutral solutions (~0.9, this study) is higher than that for Si in seawater (0.4, Savenko and Volkov, 2003) and in diluted $FeCl_2$ solutions (0.82, Schwertman and Thalmann, 1976). This comparison demonstrates the possibility of Ge versus Si fractionation during their interaction with iron hydroxide. However, specially designed comparative experiments are necessary to quantitatively resolve the fractionation factor.

It can be suggested that germanium is not conservative in natural environments where significant oxidation of Fe(II) occurs at pH > 4. There are, therefore, three main geological settings where the scavenging of Ge by the precipitation of iron oxy(hydr)oxides can induce significant changes of the Ge/Si ratio. First, the emergence of underground reduced waters is often followed by the precipitation of iron oxy(hydr)oxides in the vicinity of the spring. In such settings, the decrease of the Ge/Si ratio in the fluid induced by the preferential scavenging of Ge has already been invoked (Anders et al., 2003). Second, a redox barrier near the sediment-water interface can also yield a decrease of Ge/Si in solution. This is the case for the majority of continental margin environments, and several studies demonstrated the preferential partitioning of Ge versus Si into the solid related to the redox cycle of Fe—i.e., Ge is removed where Fe is precipitated in the sediments and remobilized at depth (Murname et al., 1989; McManus et al., 2003). A third geological setting could be the top of the hydrothermal plume above hydrothermal vents near the oceanic ridges. Few studies, carried out along the Southern Juan de Fuca Ridge, showed that the Ge/^{3}He ratios in the plume could be up to 70% lower than the same ratio in the vent (Mortlock et al., 1993). Our results show that the efficiency of Ge removal by the precipitation of iron hydroxide in hydrothermal plumes is likely to depend on the relative kinetics of oxidation and pH increase but confirm that hydrothermal plumes are potential Ge sinks.

Neutral warm Fe-rich springs ($T = 35$–38 °C, pH 6.5, $[Fe]_{aq} = 215$ μmol/L, $[Ge]_{aq} = 27.5$ nmol/L) abundant near active Karymsky volcano in Central Kamchatka can been considered as an analog of laboratory Fe precipitation. In these natural settings, Fe(II)–HCO_3^- hydrothermal solutions are rapidly degassed/oxidized at the contact with the atmosphere and form, in a short distance of 1–3 m, massive deposits of iron hydroxide without any contamination from clays or non-ferric biogenic minerals (Pokrovsky et al., unpublished). It can be seen in Fig. 9 that Ge partition coefficient measured in these springs is in reasonable agreement with that predicted from our laboratory experiments.

Another example is Ge coprecipitation with iron colloids which are formed at ambient temperatures (15–20 °C) and neutral pH (around 6–7) during groundwater/swamp and soil water discharge at the earth surface in boreal landscapes of White Sea South Coast, N. Russia (unpublished) and in the wetlands of Central Siberia on the permafrost-dominated terrain (Pokrovsky et al., 2006). Ge partition coefficient can be defined, in accord with Eq. (3), as $K_d = (Ge/Fe)_{colloidal}/(Ge/Fe)_{dissolved}$ where

"colloidal" means ultrafiltrate/dialysate fraction between 1 kDa (~1 nm) and 0.45 μm and "dissolved" represents the permeate fraction passed through 1 kDa membrane. In both cases, the K_d value is close to 0.5, which is comparable with the value 0.7 obtained in this study for Fe(II) oxidation experiments. Numerous filtrations and ultrafiltrations (5 μm → 0.22 μm → 100 kDa → 10 kDa → 1 kDa) performed on organo-ferric colloids in boreal rivers of NW Russia yield $0.1 \leqslant K_d$ (Ge/Fe) $\leqslant 0.95$ with a median value around 0.4–0.5 as calculated based on results of Pokrovsky and Schott (2002). Note that the high concentration of dissolved organic carbon (~30 mg/L) encountered in all samples of peatland waters can account for Ge complexation in solution (i.e., Pokrovski et al., 2000). This may decrease the activity of free $Ge(OH)_4^0$ in solution and thus decrease the Ge partition coefficient in natural colloids compared to organic-free laboratory experiments. At the same time, Si concentration in all ultrafiltrates remains constant thus offering a possibility of Ge/Si discrimination associated with Fe colloidal formation and transport in continental waters.

Unfortunately, due to analytical constraints, it is not possible to probe Ge speciation in natural iron hydroxides or organo-ferric colloids with low Ge/Fe ratio. We anticipate, however, an increase in the proportion of octahedral Ge in natural samples with the decrease of Ge concentration in solution. While extrapolation of our model parameters to typical natural environments should not require the change of adsorption and partitioning constants, the chemical status of Ge and related isotopic fractionation might be different between the laboratory and the field.

5. Conclusions

The present study allows quantitative characterization of Ge interactions with Fe hydroxide occurring during its adsorption on goethite and coprecipitation with $Fe(OH)_3$ at ambient temperatures. A surface complexation model developed on the basis of adsorption results is consistent with available data on other anions and neutral molecules adsorption on goethite and provides adequate description of the extent of Ge sorption as a function of pH, solid/solution ratio and Ge aqueous concentration. The dominant Ge surface complex is $>FeH_3GeO_4^0$ that is replaced by $>FeH_2GeO_4^-$ at pH above 9.5. Coprecipitation experiments with iron hydroxides allowed determination of empirical Ge partition coefficients (0.7–0.9) which is valid in a very broad range of Ge concentration (over 4 orders of magnitude). High-resolution EXAFS spectroscopy revealed essentially a tetrahedral environment with the formation of bi-dentate mononuclear (edge-sharing) and bi-dentate binuclear (double-corner-sharing) complexes at the surface of goethite and incorporated in $Fe(OH)_3$, respectively. Octahedrally coordinated Ge (30–50%) has been detected for coprecipitated samples with molar (Ge/Fe) < 0.001. In many terrestrial environments, Ge transport is likely to be controlled by iron hydroxides and organo-mineral colloids with distribution coefficients similar to those determined in the present study. Therefore, among other factors, the presence of iron hydroxides and organic matter may be responsible for Ge versus Si discrimination and Ge isotopic fractionation (i.e., Galy et al., 2002).

Acknowledgments

The manuscript greatly benefited from thorough and constructive reviews of A. Kurtz and two anonymous referees. The ESRF scientific committee is acknowledged for providing beamtime and access to the synchrotron facility. The authors are grateful to C. Causserand, F. Candadap, and J. Escalier, for the assistance with Ge analysis and J. Roux, T. Neisuis, L. Alvarez, J.-L. Hazemann, J.-J. Menthonnex, and V. Nassif for the help with XAFS. M. Thibault is thanked for carrying out XRD analyses. B. Prelot is thanked for providing goethite powder. This work was partially supported by the GDR "TRANSMET" program and by the Programme National coordoné ANR ECCO 2005.

Associate editor: James R. Rustad

Appendix A. Supplementary data

Supplementary data associated with this article can be found, in the online version, at doi:10.1016/j.gca.2006.04.012.

References

Allison, J.D., Brown, D.S., Novo-Gradac, K.J., 1991. MINTEQA2/PRODEFA2, A geochemical assessment model for environmental systems: version 3.0 user's manual. U.S. EPA, Athens, GA, 106 p.

Anders, A.M., Sletten, R.S., Derry, L.A., Hallet, B., 2003. Germanium/silicon ratios in the Copper River Basin, Alaska: weathering and partitioning in periglacial versus glacial environments. *J. Geophys. Res.* **108** (No. F1), 6005.

Ankudinov, A.L., Ravel, B., Rehr, J.J., Conradson, S.D., 1998. Real-space multiple-scattering calculation and interpretation of X-ray-absorption near-edge structure. *Phys. Rev.* **B58**, 7565–7576.

Baes Jr., C.F., Mesmer, R.E., 1976. *The Hydrolysis of Cations*. Wiley.

Barbier, J., Lévy, D., 1998. $Pb_2Fe_2Ge_2O_9$, the germanate analogue of the silicate mineral melanotekite. *Acta Cryst.* **C54**, 2–5.

Baur, W.H., Khan, A.A., 1971. Rutile-type compounds. IV. SiO_2, GeO_2 and a comparison with other rutile-type structures. *Acta Cryst.* **B27**, 2133–2139.

Bernstein, L.R., 1985. Germanium geochemistry and mineralogy. *Geochim. Cosmochim. Acta* **49**, 2409–2422.

Bernstein, L.R., Waychunas, G.A., 1987. Germanium crystal chemistry in hematite and goethite from the Apex Mine, Utah, and some new data on germanium in aqueous solution and in stottite. *Geochim. Cosmochim. Acta* **51**, 623–630.

Bibak, A., Borggaard, O.K., 1994. Molybdenum adsorption by aluminum and iron oxides and humic acid. *Soil Sci.* **158**, 323–328.

Combes, J.M., Manceau, A., Calas, G., Bottero, J.-Y., 1989. Formation of ferric oxides from aqueous solutions: a polyhedral approach by X-ray absorption spectroscopy: I. Hydrolysis and formation of ferric gels. *Geochim. Cosmochim. Acta* **53**, 583–594.

Cornell, R.M., Schwertmann, U., 1996. *The Iron: Structure, Properties, Reactions, Occurrences and Uses*. VCH, Weinheim.

Cotton, F.A., Wilkinson, G., 1966. *Advanced Inorganic Chemistry*. Wiley.
Davis, C.C., Chen, H.-W., Edwards, M., 2002. Modeling silica sorption to iron hydroxide. *Environ. Sci. Technol.* **36**, 582–587.
Derry, L.A., Kurtz, A.C., Ziegler, K., Chadwick, O.A., 2005. Biological control of terrestrial silica cycling and export fluxes to watersheds. *Nature* **433**, 728–731.
Derry, L.A., Pett-Ridge, J.C., Kurtz, A.C., Troester, J.W., 2006. Ge/Si and 87Sr/86Sr traces of weathering reactions and hydrological pathways in a tropical granitoid system. *J. Geochem. Explor.* **88**, 271–274.
Dietzel, M., 2002. Interaction of polysilicic and monosilicic acid with mineral surfaces. In: Stober, I., Bucher, K. (Eds.), *Water-Rock Interaction*. Kluwer Academic Publishers, pp. 207–235.
Dzombak, D.A., Morel, F.M.M., 1990. *Surface Complexation Modeling-Hydrous Ferric Oxide*. Wiley.
Elderfield, H., Schultz, A., 1996. Mid-ocean ridge hydrothermal fluxes and the chemical composition of the ocean. *Ann. Rev. Earth Planet. Sci.* **24**, 191–224.
Farquhar, M.L., Charnock, J.M., Livens, F.R., Vaughan, D.J., 2002. Mechanisms of arsenic uptake from aqueous solution by interaction with goethite, lepidocrocite, mackinawite, and pyrite: an X-ray absorption spectroscopy study. *Environ. Sci. Technol.* **36**, 1757–1762.
Fendorf, S., Eick, M.J., Grossl, P., Sparks, D.L., 1997. Arsenate and chromate retention mechanisms on goethite. 1. Surface structure. *Environ. Sci. Technol.* **31**, 315–320.
Filippelli, G.M., Carnahan, J.W., Derry, L.A., Kurtz, A., 2000. Terrestrial paleorecords of Ge/Si cycling derived from lake diatoms. *Chem. Geol.* **168**, 9–26.
Filius, J.D., Hiemstra, T., Van Riemsdijk, W.H., 1997. Adsorption of small weak organic acids on goethite: modeling of mechanisms. *J. Colloid Interface Sci.* **195**, 368–380.
Froelich, P.N., Hambrick, G.A., Andreae, M.O., Mortlock, R.A., Edmond, J.M., 1985. The geochemistry of inorganic germanium in natural waters. *J. Geophys. Res.* **90**, 1133–1141.
Froelich, P.N., Blanc, V., Mortlock, R.A., Chilrud, S.N., Dunstan, W., Udomkit, A., Peng, T.H., 1992. River fluxes of dissolved silica to the ocean were higher during glacials: Ge/Si in diatoms, rivers, and oceans. *Paleoceanography* **7**, 739–767.
Fuller, C.C., Dadis, J.A., Waychunas, G.A., 1993. Surface chemistry of ferrihydrite: Part 2. Kinetics of arsenate adsorption and coprecipitation. *Geochim. Cosmochim. Acta* **57**, 2271–2282.
Galy A., Pokrovsky O.S., Schott J. (2002) Ge-isotopic fractionation during its sorption on goethite: an experimental study. Abstracts of the VM Goldschmidt Conference. August 18–23, 2002, Davos, Switzerland. Suppl. *Geochim. Cosmochim. Acta*, **66** p. A259.
Glasauer, S., Friedl, J., Schwertmann, U., 1999. Properties of goethites prepared under acidic and basic conditions in the presence of silicate. *J. Colloid Interface Sci.* **216**, 106–115.
Goldberg, S., Forster, H.S., Godfrey, C.L., 1996. Molybdenum adsorption on oxides, clay minerals and soils. *Soil Sci. Soc. Am. J.* **60**, 425–432.
Goldschmidt, V.M., 1958. *Geochemistry*. Oxford University Press.
Grafe, M., Eick, M.J., Grossl, P.R., 2001. Adsorption of arsenate(V) and arsenite(III) on goethite in the presence and absence of dissolved organic carbon. *Soil Sci. Soc. Am. J.* **65**, 1680–1687.
Harrison, J.B., Berkheiser, V.E., 1982. Anion interactions with freshly prepared hydrous iron oxides. *Clays Clay Minerals* **30**, 97–102.
Hiemstra, T., Van Riemsdijk, W.H., 1999. Surface structural ion adsorption modeling of competitive binding of oxyanions by metal (hydr)oxides. *J. Colloid Interface Sci.* **210**, 182–193.
Jorgensen, J.D., 1978. Compression mechanism in α-quartz structure: SiO_2 and GeO_2. *J. Appl. Phys.* **49**, 5473–5478.
King, S.L., Froelich, P.N., Jahnke, R.A., 2000. Early diagenesis of germanium in sediments of the Antartic South Atlantic: in search of the missing Ge sink. *Geochim. Cosmochim. Acta* **64**, 1375–1390.
Kurtz, A.C., Derry, L.A., Chadwick, O.A., 2002. Germanium-silicon fractionation in the weathering environment. *Geochim. Cosmochim. Acta* **66**, 1525–1537.
Machesky, M.L., Brian, L., Bischoff, B.L., Anderson, M.A., 1989. Calorimetric investigation of anion adsorption onto goethite. *Environ. Sci. Technol.* **23**, 580–587.
Machesky, M.L., Wilson, O., Andrade, W.O., Rosea, A.W., 1991. Adsorption of gold(III)-chloride and gold(I)-thiosulfate anions by goethite. *Geochim. Cosmochim. Acta* **55**, 769–776.
Manceau, A., 1995. The mechanism of anion adsorption on iron oxides: evidence for the bonding of arsenate tetrahedra on free $Fe(O,OH)_6$ edges. *Geochim. Cosmochim. Acta* **59**, 3647–3653.
Manceau, A., Combes, J.M., 1988. Structure of Mn and Fe oxides and oxy-hydroxides: a topological approach by EXAFS. *Phys. Chem. Minerals* **15**, 283–295.
Manceau, A., Charlet, L., 1994. The mechanism of selenate adsorption on goethite and hydrous ferric oxide. *J. Colloid Interface Sci.* **168**, 87–93.
Manning, B.A., Fendorf, S.E., Goldberg, S., 1998. Surface structures and stability of arsenic(III) on goethite: Spectroscopic evidence for inner-sphere complexes. *Environ. Sci. Technol.* **32**, 2383–2388.
McManus, J., Hammond, D.E., Cummins, K., Klinkhammer, G.K., Berelson, W.M., 2003. Diagenetic Ge–Si fractionantion in continental margin environments: further evidence for a nonopal Ge sink. *Geochim. Cosmochim. Acta* **67**, 4545–4557.
Mortlock, R.A., Froelich, P.N., 1987. Continental weathering of germanium: Ge/Si in the global river discharge. *Geochim. Cosmochim. Acta* **51**, 2075–2082.
Mortlock, R.A., Froelich, P.N., Feely, R.A., Massoth, G.J., Butterfield, D.A., Lupton, J.E., 1993. Silica and germanium in Pacific Ocean hydrothermal vents and plumes. *Earth Planet. Sci. Lett.* **119**, 365–378.
Munoz, M., Argoul, P., Farges, F., 2003. Continuous Cauchy wavelet transform analyses of EXAFS spectra: a qualitative approach. *Am. Miner.* **88**, 694–700.
Murname, R.J., Leslie, B., Hammond, D.E., Stallard, R.F., 1989. Germanium geochemistry in the southern California borderlands. *Geochim. Cosmochim. Acta* **53**, 2873–2882.
Murname, R.J., Stallard, R.F., 1990. Germanium and silicon in rivers of the Orinoco drainage basin. *Nature* **344**, 749–752.
Newville, M., 2001. IFEFFIT: interactive XAFS analysis and FEFF fitting. *J. Synchrotron Radiat.* **8**, 322–324.
Nishi, F., Takéuchi, Y., 1992. The nature and variation of Ge–O bonding in germanates. *Zeit. Kristallogr.* **202**, 251–259.
O'Reilly, S.E., Strawn, D.G., Sparks, D.L., 2001. Residence time effects on arsenate adsorption/desorption mechanisms on goethite. *Soil Sci. Soc. Am. J.* **65**, 67–77.
Pazenkova, N.I., 1967. Germaniferous limonite-forming mechanism. *Doklady Acad. Sci. USSR, Earth Sci. Sections* **173**, 204–206, English translation.
Pivovarov, S., 1997. Surface structure and site density of the oxide-solution interface. *J. Colloid Interface Sci.* **196**, 321–323.
Poiarkova A.V. (1999) X-ray absorption fine structure Debye-Waller factors. *Ph.D. thesis, University of Washington.*
Poiarkova, A.V., Rehr, J.J., 1999. Multiple-scattering X-ray-absorption fine-structure Debye-Waller factor calculations. *Phys. Rev. B* **59**, 948–957.
Pokrovski, G.S., Schott, J., 1998a. Thermodynamic properties of aqueous Ge(IV) hydroxide complexes from 25 to 350 °C: implications for the behavior of germanium and the Ge/Si ratio in hydrothermal fluids. *Geochim. Cosmochim. Acta* **62**, 1631–1642.
Pokrovski, G.S., Schott, J., 1998b. Experimental study of the complexation of silicon and germanium with aqueous organic species: implications for germanium and silicon transport and Ge/Si ratio in natural waters. *Geochim. Cosmochim. Acta* **62**, 3413–3428.
Pokrovski, G.S., Martin, F., Hazemann, J.-L., Schott, J., 2000. An X-ray absorption fine structure spectroscopy study of germanium-organic ligand complexes in aqueous solution. *Chem. Geol.* **163**, 151–165.
Pokrovski, G.S., Schott, J., Farges, F., Hazemann, J-L., 2003. Iron(III)-silica interactions in aqueous solution: insights from X-ray absorption fine structure spectroscopy. *Geochim. Cosmochim. Acta* **67**, 3559–3573.
Pokrovski, G.S., Roux, J., Hazemann, JL., Testemale, D., 2005. An X-ray Absorption spectroscopy study of argutite solubility and germanium

aqueous speciation in hydrothermal fluids to 500 °C and 400 bar. *Chem. Geol.* **217**, 127–145.

Pokrovsky, O.S., Schott, J., 2002. Iron colloids/organic matter associated transport of major and trace elements in small boreal rivers and their estuaries (NW Russia). *Chem. Geol.* **190**, 141–179.

Pokrovsky, O.S., Pokrovski, G.S., Schott, J., 2004. Gallium(III) adsorption on carbonates and oxides: X-ray absorption fine structure spectroscopy and surface complexation modelling. *J. Colloid Interface Sci.* **279**, 314–325.

Pokrovsky, O.S., Pokrovski, G.S., Gélabert, A., Schott, J., Boudou, A., 2005. Speciation of zinc associated with diatoms using X-ray absorption spectroscopy. *Environ. Sci. Technol.* **39**, 4490–4498.

Pokrovsky, O.S., Schott, J., Dupré, B., 2006. Basalt weathering and trace elements migration in boreal Arctic zone. *J. Geochem. Explor.* **88**, 304–307.

Ravel, B., Newville, M., 2005. ATHENA, ARTEMIS, HEPHAESTUS: data analysis for X-ray absorption spectroscopy using IFEFFIT. *J. Synchronron Radiat.* **12**, 537–541.

Rietra, R.P.J.J., Hiemstra, T., Willem, H., Van Riemsdijk, W.H., 2001. Comparison of selenate and sulfate adsorption on goethite. *J. Colloid Interface Sci.* **240**, 384–390.

Ross II, C.R., Bernstein, L.R., Waychunas, G.A., 1988. Crystal-structure refinement of stottite, $FeGe(OH)_6$. *Am. Miner.* **73**, 657–661.

Rustad, J.R., Hay, B.P., 1995. A molecular dynamics study of solvated orthosilicic acid and orthosilicate anion using parameterized potentials. *Geochim. Cosmochim. Acta* **59**, 1251–1257.

Savenko, A.V., 1995. Coprecipitation of phosphorus with iron hydroxide formed during mixing of submarine hydrothermal fluids with seawater. *Geochem. Int.* **No. 9**, 1383–1389.

Savenko, A.V., 1996. Aluminum behavior during the process of hydrothermal solutions mixing with the seawater: data of experimental modeling. *Oceanology* **3** (No 5), 735–740.

Savenko, A.V., 1998. Coprecipitation of phosphorus, arsenic and vanadium with iron hydroxide in hydrothermal plumes. *Dokl. Acad. Sci. Russ.* **36** (No 5), 679–681.

Savenko, A.V., 1999a. Experimental modeling of oxyanions (PO_4^{3-}, VO_4^{3-}, CrO_4^{3-}, AsO_3^{3-}, AsO_4^{3-}) with iron hydroxide in hydrothermal plumes. *Geochem. Int.* **No. 3**, 281–288.

Savenko, A.V., 1999b. On the mechanism of mercury accumulation in metalliferous oceanic sediments. *Geochem. Int.* **No. 9**, 1022–1024.

Savenko, A.V., 2000. On the mechanism of boron accumulation in metalliferous oceanic sediments. *Oceanology* **4** (No. 2), 217–220.

Savenko, A.V., Volkov, I.I., 2003. On the abiogenic precipitation of silica in the modern ocean. *Geochem. Int.* **No. 6**, 676–680.

Schwertman, U., Thalmann, H., 1976. The influence of [Fe(II)], [Si], and pH on the formation of lepidocrocite and ferrihydrite during oxidation of aqueous $FeCl_2$ solutions. *Clay Minerals* **11**, 189–200.

Shemesh, A., Mortlock, R.A., Froelich, P.N., 1989. Late Cenozoic Ge/Si record of marine biogenic opal: Implications for variations in riverine fluxes to the ocean. *Paleoceanography* **4**, 221–234.

Tréguer, P., Nelson, D.M., van Bennekom, A.J., DeMaster, D.J., Laynaert, A., Quéguiner, B., 1995. The silica balance in the world ocean: a re-estimate. *Science* **268**, 375–379.

Vempati, R.K., Loeppert, R.H., 1989. Influence of structural and adsorbed Si on the transformation of synthetic ferrihydrite. *Clays Clay Minerals* **37**, 273–279.

Viers, J., Dupré, B., Polvé, M., Schott, J., Dandurand, J.-L., Braun, J.-J., 1997. Chemical weathering in in the drainage basin of a tropical watershed (Nsimi-Zoétélé site, Cameroon). *Chem. Geol.* **140**, 181–206.

Viollier, R., Inglett, P.W., Hunter, K., Roychoudhury, A.N., Van Cappellen, P., 2000. The ferrozine method revisited: Fe(II)/Fe(III) determination in natural waters. *Appl. Geochem.* **15**, 785–790.

Waychunas, G.A., Rea, B.A., Fuller, C.C., Davis, J.A., 1993. Surface chemistry of ferrihydrate: Part 1. EXAFS studies of the geometry of coprecipitated and adsorbed arsenate. *Geochim. Cosmochim. Acta* **57**, 2251–2269.

Wyckoff R.W.G. (1963) *Crystal Structures.* vol. 1, second ed.. Interscience Publishers, New York, pp. 290–295.

Yoshiasa, A., Tamura, T., Kamishima, O., Murai, K., Ogata, K., Mori, H., 1999. Local structure and mean-square relative displacement in SiO_2 and GeO_2 polymorphs. *J. Synchrotron Radiat.* **6**, 1051–1058.

Zhou, L., Kyte, F.T., 1991. Are there any significant sinks in the marine Ge cycle other than biogenic opal? *Eos* **72**, 263–264 (abstr.).